NAVAL SHIP RESEARCH AND DEVELOPMENT CENTER
Washington, D.C. 20034

DROP TESTS OF CONES TO INVESTIGATE THE THREE-DIMENSIONAL EFFECTS OF SLAMMING

by

Sheng-Lun Chuang and
David T. Milne

DEPARTMENT OF STRUCTURAL MECHANICS
RESEARCH AND DEVELOPMENT REPORT

[redacted]

April 1971 Report 3543

Report 3543
DROP TESTS OF CONES TO INVESTIGATE THE THREE-DIMENSIONAL EFFECTS OF SLAMMING

The Naval Ship Research and Development Center is a U.S. Navy center for laboratory effort directed at achieving improved sea and air vehicles. It was formed in March 1967 by merging the David Taylor Model Basin at Carderock, Maryland and the Marine Engineering Laboratory (now Naval Ship R & D Laboratory) at Annapolis, Maryland. The Mine Defense Laboratory (now Naval Ship R & D Laboratory) Panama City, Florida became part of the Center in November 1967.

Naval Ship Research and Development Center
Washington, D.C. 20034

MAJOR NSRDC ORGANIZATIONAL COMPONENTS

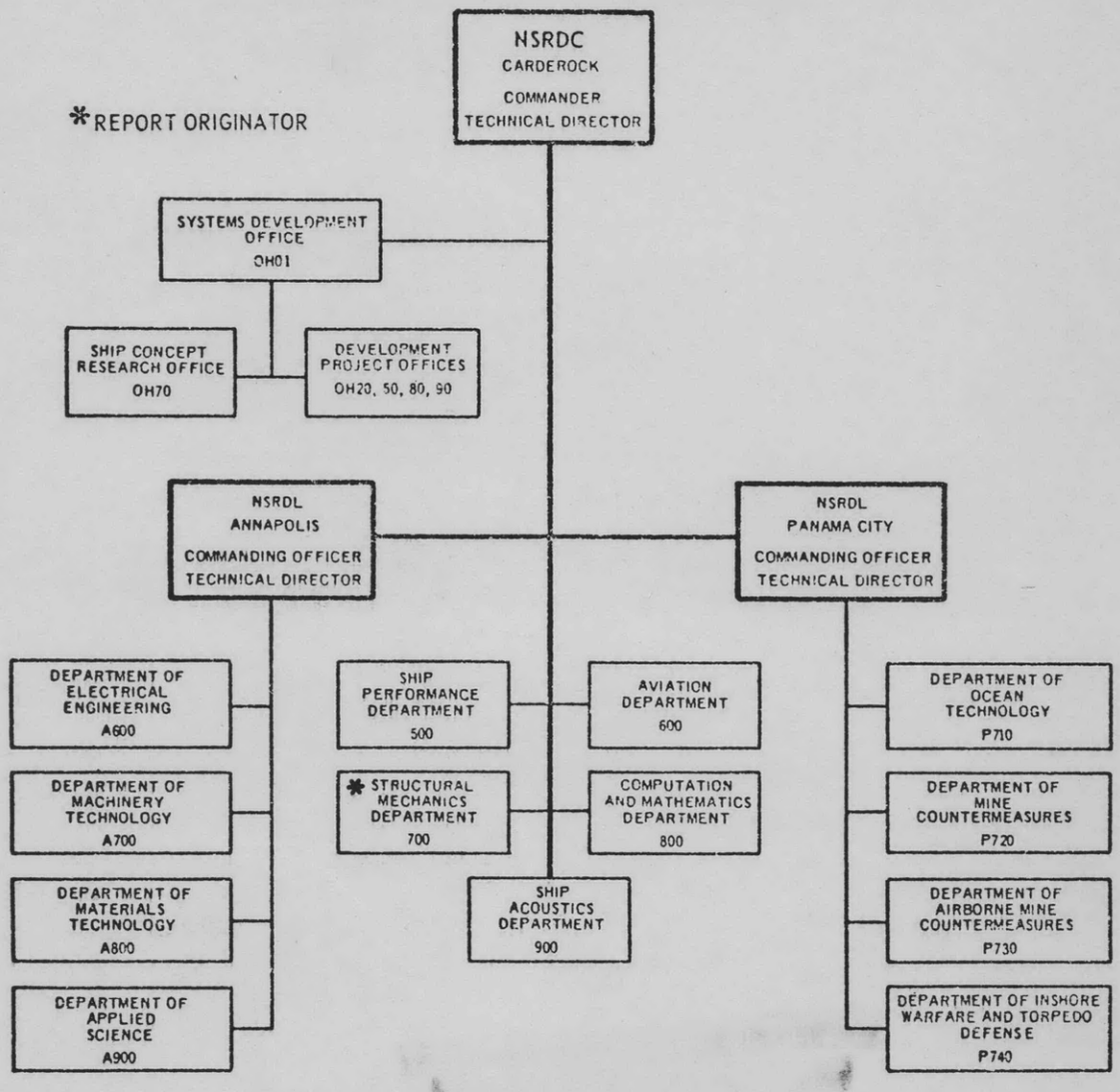

DEPARTMENT OF THE NAVY
NAVAL SHIP RESEARCH AND DEVELOPMENT CENTER
WASHINGTON, D. C. 20034

DROP TESTS OF CONES TO INVESTIGATE THE THREE-DIMENSIONAL EFFECTS OF SLAMMING

by

Sheng-Lun Chuang and
David T. Milne

April 1971

Report 3543

TABLE OF CONTENTS

LIST OF FIGURES

NOTATION

c	Capacitance
g	Acceleration due to gravity
k	Arbitrary constant
n	Arbitrary constant
P-P	Peak to peak
p	Impact pressure in pounds per square inch
p_{max}	Maximum impact pressure in pounds per square inch
Q, q	Charge in coulombs
V	Impact velocity in feet per second
V, v	Voltage in volts
VP	Peak voltage in volts
w	Weight per unit volume in pounds per cubic foot
ρ	Mass density of fluid (= w/g)

ABSTRACT

Rigid-body slamming was experimentally investigated at the Naval Ship Research and Development Center by dropping one flat circular aluminum plate model and five cone-shaped aluminum models with small deadrise angles (up to 15 deg) from various elevated positions above a calm water surface. This report presents the test results and compares them with theory and to those for two-dimensional wedge-shaped models.

ADMINISTRATIVE INFORMATION

This investigation was carried out as part of a general study on slamming. The work was funded jointly by Subproject S46-06X, Task 1707 (Hydrofoil Hull) and by JSESPO. However, the publication of this report was funded by JSESPO alone.

INTRODUCTION

The two-dimensional impact test of a rigid flat-bottom model indicated that the maximum impact pressure is nowhere near the theoretical infinitely large hydrodynamic pressure nor near the theoretical acoustic pressure.[1] The cushioning effect of the compressible air trapped between the impact body and the water surface reduces the maximum impact pressure to about one-tenth of the acoustic pressure. However, the nature of the trapped air phenomenon is not very stable. Much more air is trapped for the impact of a flat bottom and a 1-deg wedge than for wedges with deadrise angles of 3 deg or higher.

Tests of elastic models verified the fact that the pressure generated by the impact is affected by the vibratory movement of the impact surface and that it can be separated into rigid body impact pressure and interacting pressure.[1] This dynamic interaction is closely related to the hydrodynamic phenomenon rather than to the acoustic phenomenon.

Past studies have therefore demonstrated that in the two-dimensional impact of rigid and elastic bodies (1) water can be treated as an

---

[1]References are listed on page 40.

incompressible fluid regardless of the size of the deadrise angle of the wedge, (2) trapped air must be taken into consideration for small deadrise angles, and (3) the structural response to impact can be treated as the impact of a deformable body on an incompressible fluid, with or without trapped air.

As a consequence of these findings, questions naturally arose regarding the three-dimensional effect of slamming and led to the series of drop tests of cone-shaped models discussed herein. In order to compare two- and three-dimensional impact phenomena, drop tests of a two-dimensional flat-bottom model were repeated, and test data of wedge-shaped models were reanalyzed. A theoretical investigation on slamming of cone-shaped bodies was also performed; results are presented elsewhere.[2]

The objective of the present study is therefore to investigate the three-dimensional effects of slamming from the drop tests of wedges and cones. To fulfill this objective, the trapped air phenomenon and pressure time histories are compared for these series of tests.

The measurement of transient pressure requires instrumentation of a specialized nature. Appendix A of the report is devoted to a description of instrumentation, features of circuit designs, calibration techniques, and operational procedures. To utilize the General Electric Computer Time-Sharing System, a small program was written to fit the test results by the method of least squares. This program is presented in Appendix B.

Drop tests of cone-shaped models were performed at the Center during Fiscal Year 1969.

METHOD

DESCRIPTION OF MODELS FOR STUDYING THREE-DIMENSIONAL EFFECTS

The six 16-in.-diameter aluminum models consisted of a flat circular plate with 0-deg deadrise angle and five cone shapes with deadrise angles of 1, 3, 6, 10, and 15 deg. The impact surfaces of the models were machine-finished to ensure smoothness and true conical configuration.

TEST PROCEDURE

Tests were conducted in a 25- by 15-ft rectangular tank which was filled with water to a depth of 7 ft 2 in.

Details of the test assembly are shown in Figure 1. The releasing mechanism consisted of a solenoid attached to a cross beam by an adjustable steel rod which can be raised and lowered for the proper drop height of the model. The solenoid was equipped with a hook for hanging the model. When the solenoid was activated, the hook was very quickly released and the model fell freely in the vertical direction. The total drop weight of the assembly shown in the figure was 63 lb.

The drop heights (defined as the distance between the vertex of the cone and the water surface) ranged from 3 to 15 in. in 3-in. increments. Pressures, accelerations, vertical displacement, and velocities of the moving model were recorded. In addition, 16-mm high-speed underwater movies were taken to study the trapped air phenomenon during and after the impact. The film speed varied up to about 1000 frames per sec for the study.

The instrumentation system used for the experiment consisted essentially of quartz-crystal transducers, charge amplifiers, d-c amplifiers, and a tape recorder. The validity of the pressure measurements of the complete recording system was tested electronically and mechanically; the system was also calibrated by means of an underwater explosion. The results indicated that the entire recording system had the ability to pick up and record any high-frequency acoustic pressure existing during the impact of the falling body with the water surface.[3] The detailed description of instrumentation is given in Appendix A.

ADDITIONAL DATA UTILIZED

Reanalyzed test data on rectangular flat-bottom and wedge-shaped models were utilized for comparison with results of the cone-shaped models. Details of procedure and analysis are available in Reference 4.

DIFFERENCE BETWEEN TEST SETUPS OF CONE-SHAPED MODELS AND WEDGE-SHAPED MODELS

The rectangular flat-bottom and wedge-shaped models were tested in the 25 by 15 ft rectangular tank with two parallel walls to ensure two-dimensional flow conditions. These two parallel walls, made of steel plates, were constructed to span the length of the tank and to extend from 18 in. above the water surface to the full tank depth. They were rigidly connected to the tank floor and sides and were separated by a distance equal to the model length of 26 1/2 in. plus a small amount of clearance. These parallel walls had open ends to permit free flow of the surface wave around the tank during the drop test.

The cone-shaped and circular-plate models were tested in the same tank but without these parallel walls so that the flow of air and water was not restricted.

THREE-DIMENSIONAL EFFECT ON TRAPPED AIR

High-speed, 16-mm underwater movies of the drops of wedge-shaped and cone-shaped models revealed that only the 0- and the 1-deg deadrise-angle configurations of both shapes trapped a considerable amount of air and pushed some of it into the surface layer of water. Most of the air was not trapped at the instant of impact by either shape with deadrise angles of 3 deg and higher. During the impact, the higher the deadrise angle of both the wedge and the cone, the clearer and cleaner was the view of the impact surface. However, for the same deadrise angle, the wedge trapped more air than did the cone. This phenomenon is illustrated by the underwater photographs shown in Figures 2 and 3.

The fact that the three-dimensional (cone-shaped) body allowed the trapped air to escape earlier than did the two-dimensional (wedge-shaped) body was evident in comparisons of the detection of air trapped between the impact surface of the falling model and the water surface; see Figures 4 and 5. The method used to detect trapped air is given in Reference 4. The record for the wedge impact showed that only after the first positive pulse of the impact pressure was completely over did the trapped air appear partly to have escaped and partly to have been pushed

into the surface layer of water. However, the record for the cone impact showed that the trapped air began to escape or to be pushed through the water surface during the first positive pulse of the impact pressure. Because of this difference, their impact pressure time histories were affected, especially for the impact of the 1-deg wedge and cone. This will be discussed further in the next section.

THREE-DIMENSIONAL EFFECT ON IMPACT PRESSURE

The pressure time histories of the two-dimensional and three-dimensional impacts were affected because of differences in the time required for trapped air to escape. These differences can be observed in Figures 4 to 7. The shape of the pressure time histories were very much alike except for the 1-deg models, where the three-dimensional effect on the escape time of the trapped air reduced the cushioning effect of the air. Thus, the appearance of the impact pressure time histories of the 1-deg cone is similar to those of cones with higher deadrise angles, but the appearance of the impact pressure time histories of the 1-deg wedge closely resembles those of the two-dimensional flat-bottom model.

The maximum impact pressures for both shapes of models are plotted on the log-log charts shown in Figures 8 and 9. As shown in these figures, the data recorded for the wedge-shaped models were much less repeatable than those of the cone-shaped models because of improvements in the drop mechanism and the instrumentation system used for the cone-shaped models. The pressure-velocity relations were obtained empirically from test data by fitting straight lines on the charts with a general form of

$$p = k\, V^n$$

where k and n are the arbitrary constants and n has limits of $1 \leq n \leq 2$.

The method just described provides equations to estimate the maximum impact pressures of wedges and cones penetrating a water surface; they are summarized as follows:

1. Two-Dimensional Wedges and Flat Bottom:

   a. Flat bottom (20 in. wide):

      At center: $p_{max} = 0.443 \rho V^2$

      6 11/16 in. off center: $p_{max} = 0.376 \rho V^2$

   b. 1-deg wedge:

      Away from keel: $p_{max} = 0.515 \rho V^2$

   c. 3-deg wedge:

      Away from keel: $p_{max} = 0.387 \rho V^2$

   d. 6-deg wedge:

      Away from keel: $p_{max} = 0.387 \rho V^2$

   e. 10-deg wedge:

      Away from keel: $p_{max} = 0.186 \rho V^2$

   f. 15-deg wedge:

      Away from keel: $p_{max} = 0.103 \rho V^2$

2. Three-Dimensional Cones and Circular Plate:

   a. Circular plate:

      At center: $p_{max} = 0.345 \rho V^{1.96}$

      4 in. off center: $p_{max} = 0.304 \rho V^{1.90}$

   b. 1-deg cone:

      Away from vertex: $p_{max} = 2.387 \rho V^{1.60}$

   c. 3-deg cone:

      Away from vertex: $p_{max} = 0.778 \rho V^{1.83}$

   d. 6-deg cone:

      Away from vertex: $p_{max} = 0.366 \rho V^{1.84}$

   e. 10-deg cone:

      Away from vertex: $p_{max} = 0.160 \rho V^{1.91}$

   f. 15-deg cone:

      Away from vertex: $p_{max} = 0.129 \rho V^{1.70}$

The formulas for the wedges are from Reference 1 with slight revisions. The formulas for the flat bottom were obtained from a recent test, which is believed to be better than the previous tests, by using the method of least squares given in Appendix B. The formulas for the cones and circular plate were also obtained from a recent test by the method of least squares.

If test results of the cones and circular plate are forced to fit into velocity-square relations as were those for two-dimensional wedges and flat bottom models, the formulas for them are:

a. Circular plate:

At center: $p_{max} = 0.320 \rho V^2$

4 in. off center: $p_{max} = 0.258 \rho V^2$

b. 1-deg cone:

Away from vertex: $p_{max} = 1.160 \rho V^2$

c. 3-deg cone:

Away from vertex: $p_{max} = 0.562 \rho V^2$

d. 6-deg cone:

Away from vertex: $p_{max} = 0.273 \rho V^2$

e. 10-deg cone:

Away from vertex: $p_{max} = 0.134 \rho V^2$

f. 15-deg cone:

Away from vertex: $p_{max} = 0.072 \rho V^2$

Comparison of test results for the wedges and cones indicated that the maximum impact pressures were generally lower for the three-dimensional impact; see Table 1. However, because of the reduced cushioning effect of trapped air (see and compare pressure time histories of 1-deg wedges and 1-deg cones shown in Figures 6 and 7), the maximum impact pressures of the 1-deg cone were higher than those of the 1-deg wedge. For comparison, the equations just listed and theories of two wedges and cones[1,2] are also plotted in Figures 8 and 9. Since the cushioning effect of the trapped air is gradually reduced as the deadrise angle is increased, the theoretical

and the experimental maximum impact pressures at the same impact velocity are much closer in magnitude for the higher deadrise angles of wedges and cones than for the lower deadrise angles.

TABLE 1

Comparisons of k Values in Wedge and Cone Impact Pressure Empirical Formulas

Deadrise Angle deg	k values in formula $p_{max} = k\rho V^2$		
	Cone	Wedge	Cone/Wedge
Flat (center)	0.320	0.443	0.72
1	1.160	0.515	2.25
3	0.562	0.887	0.64
6	0.273	0.387	0.71
10	0.134	0.186	0.72
15	0.072	0.103	0.70

SUMMARY OF FINDINGS

Previous studies on slamming at the NSRDC Department of Structural Mechanics involved tests for two-dimensional cases. The present study extended the investigation to the three-dimensional aspect and studied its effects on slamming.

Drop tests were conducted on six aluminum models having conical impact surfaces with respective deadrise angles of 0 (circular plate), 1, 3, 6, 10, and 15 deg (see Figure 1). On the basis of this series of experimental investigations, the following conclusions are drawn:

1. During the rigid-body impact of the circular plate, the first positive pulse of the impact pressure occurs at the time when the trapped air begins to escape (Figure 5). Only the circular plate and the 1-deg cone trap considerable amounts of air; cones with deadrise angles of 3 deg and higher do not trap very much air (Figure 3).

2. The maximum impact pressures are generally about 30 percent lower for the cone than for the wedge (Figure 8).

3. Because the trapped air escaped more quickly after impact by the cone than by the wedge shape, the pressure time histories for the 1-deg cone closely resemble hydrodynamic impact rather than impact with cushioning air (see Figure 7). In contrast, the pressure time histories for 1-deg wedge resemble impact with cushioning air (see Figure 6). Thus, the maximum impact pressures of the 1-deg cone are higher than those of the 1-deg wedge (Figure 8).

ACKNOWLEDGMENTS

The authors express their thanks to Messrs. A.B. Stavovy, L.A. Becker, and G.O. Thomas who initiated this fundamental study and provided expert advice to the authors. The instrumentation system was developed under the supervision of Mr. G.W. Cook. Tests were performed with the assistance of Messrs. P. Yarnall, Jr. and N.J. Tuholski. The motion picture photography was performed by Mr. B.C. Ball, and the computer program was performed with the assistance of Mr. J.J. Ogelsby. The authors gratefully acknowledge their helpful assistance and valuable suggestions. Appreciation is also expressed to Mr. D.J. Clark and Dr. M.E. Lunchick for their support and every possible assistance in the evaluation of cone impact theory by this series of experiment.

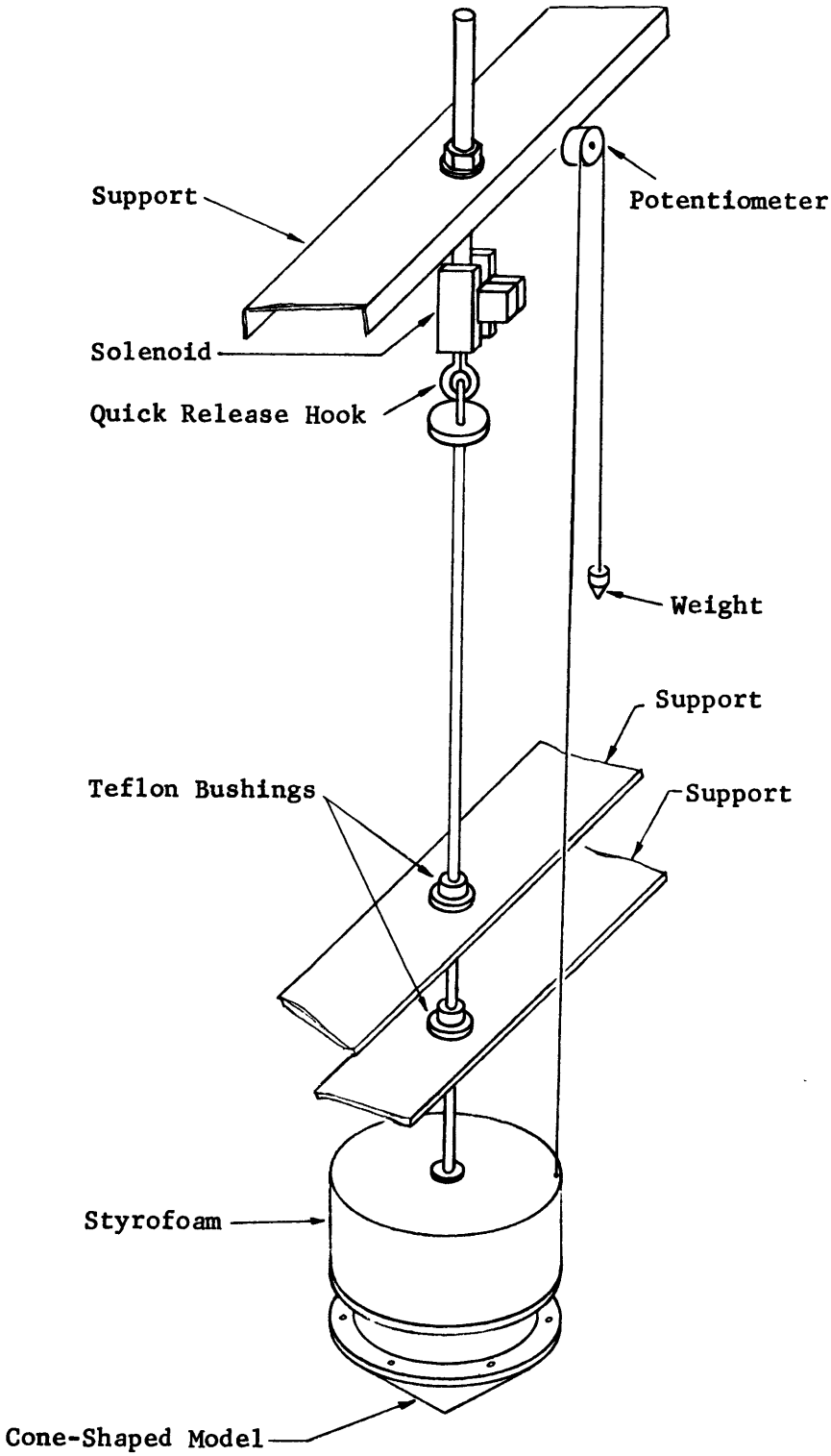

Figure 1 - Installation of Cone-Shaped Model

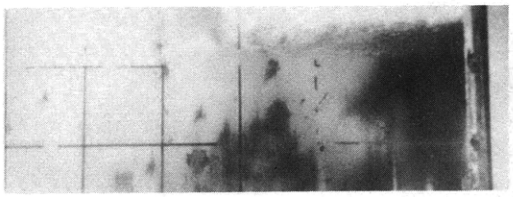

Rectangular Plate

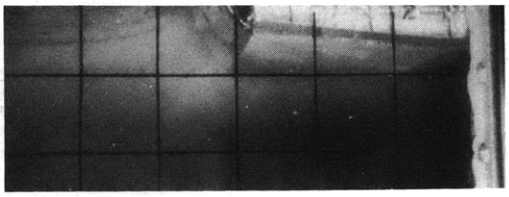

6-Deg Wedge

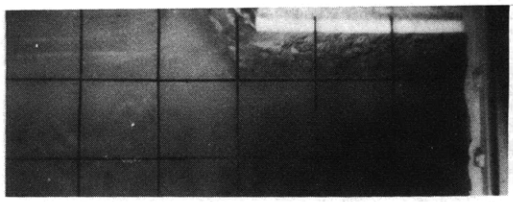

1-Deg Wedge

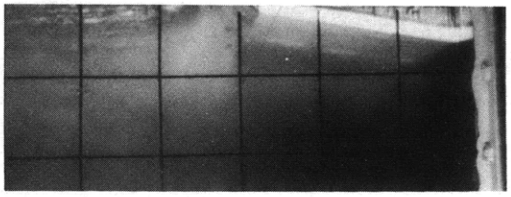

10-Deg Wedge

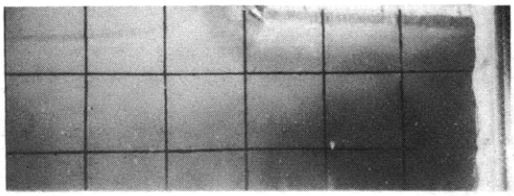

3-Deg Wedge

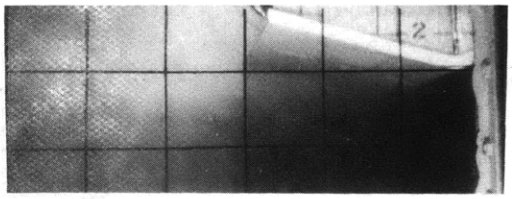

15-Deg Wedge

Figure 2 - Detection of Trapped Air during Drop Tests of Rigid Wedge-Shaped Models

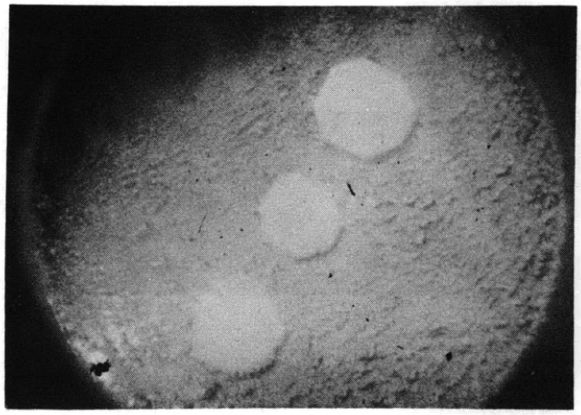

Circular Plate

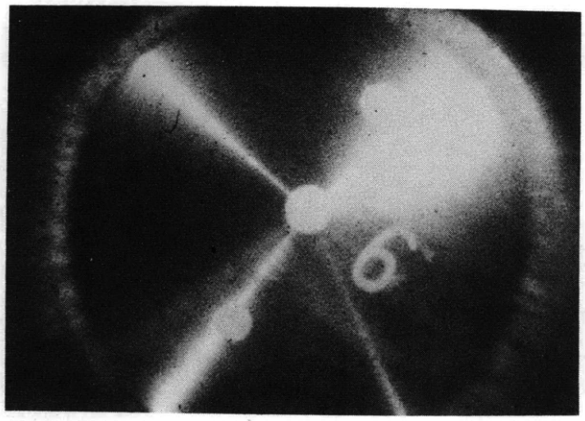

6-Deg Cone

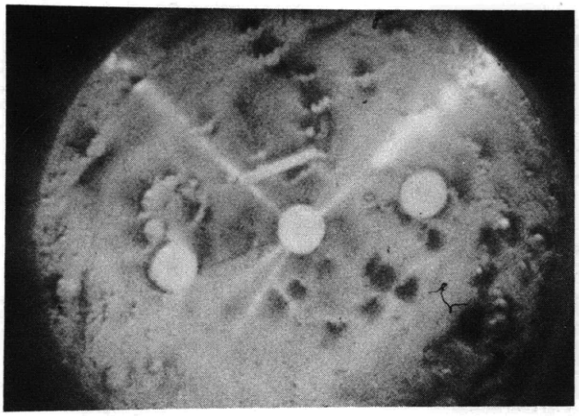

1-Deg Cone

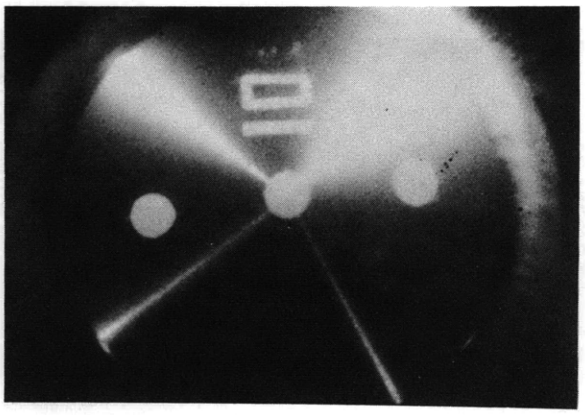

10-Deg Cone

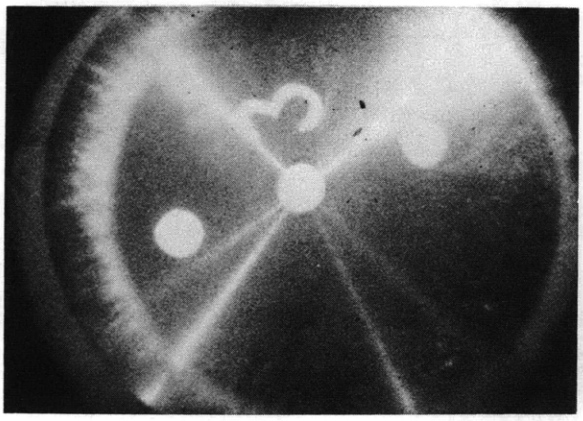

3-Deg Cone

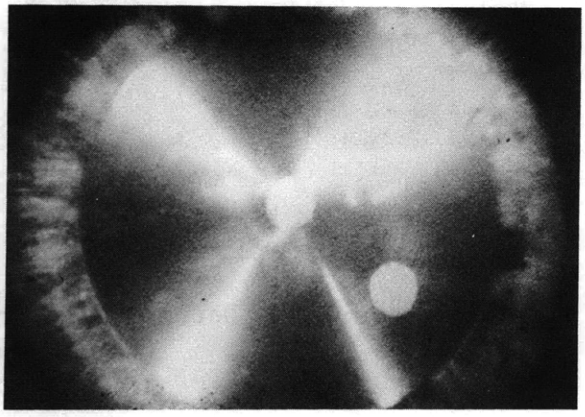

15-Deg Cone

Figure 3 - Detection of Trapped Air during Drop Tests of Rigid Cone-Shaped Models

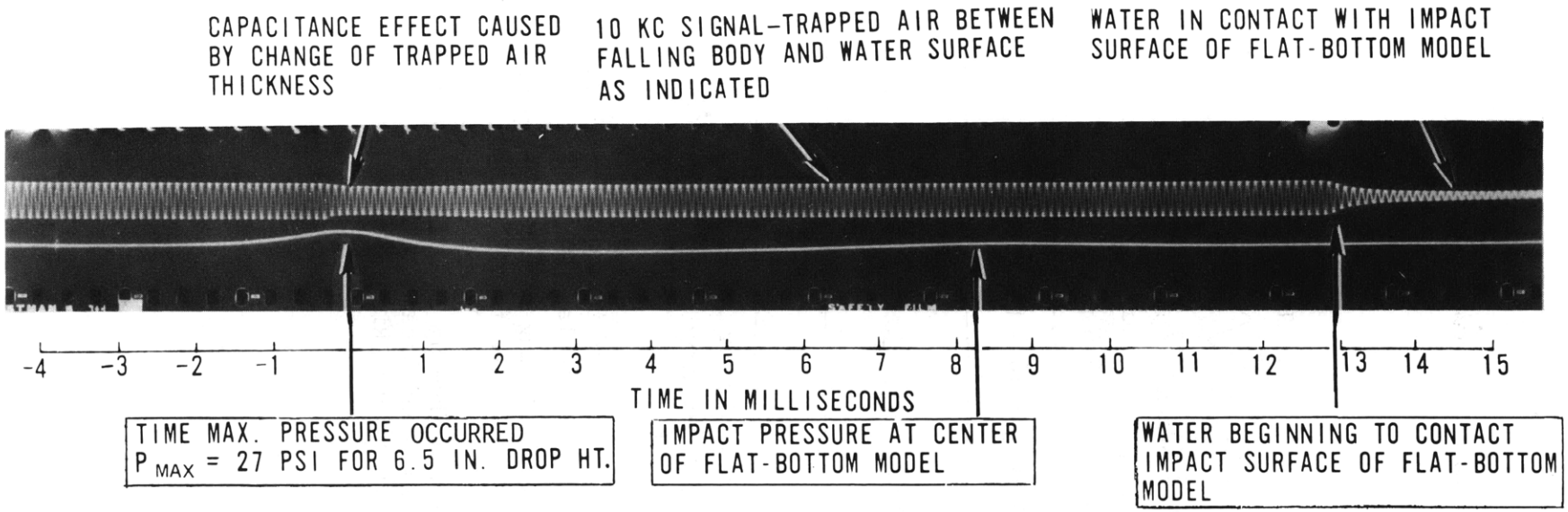

Figure 4 - Sample Record Showing Time Lag between Pulse of Maximum Impact Pressure and Escape of Trapped Air for Impact of Two-Dimensional Rigid Flat-Bottom Model

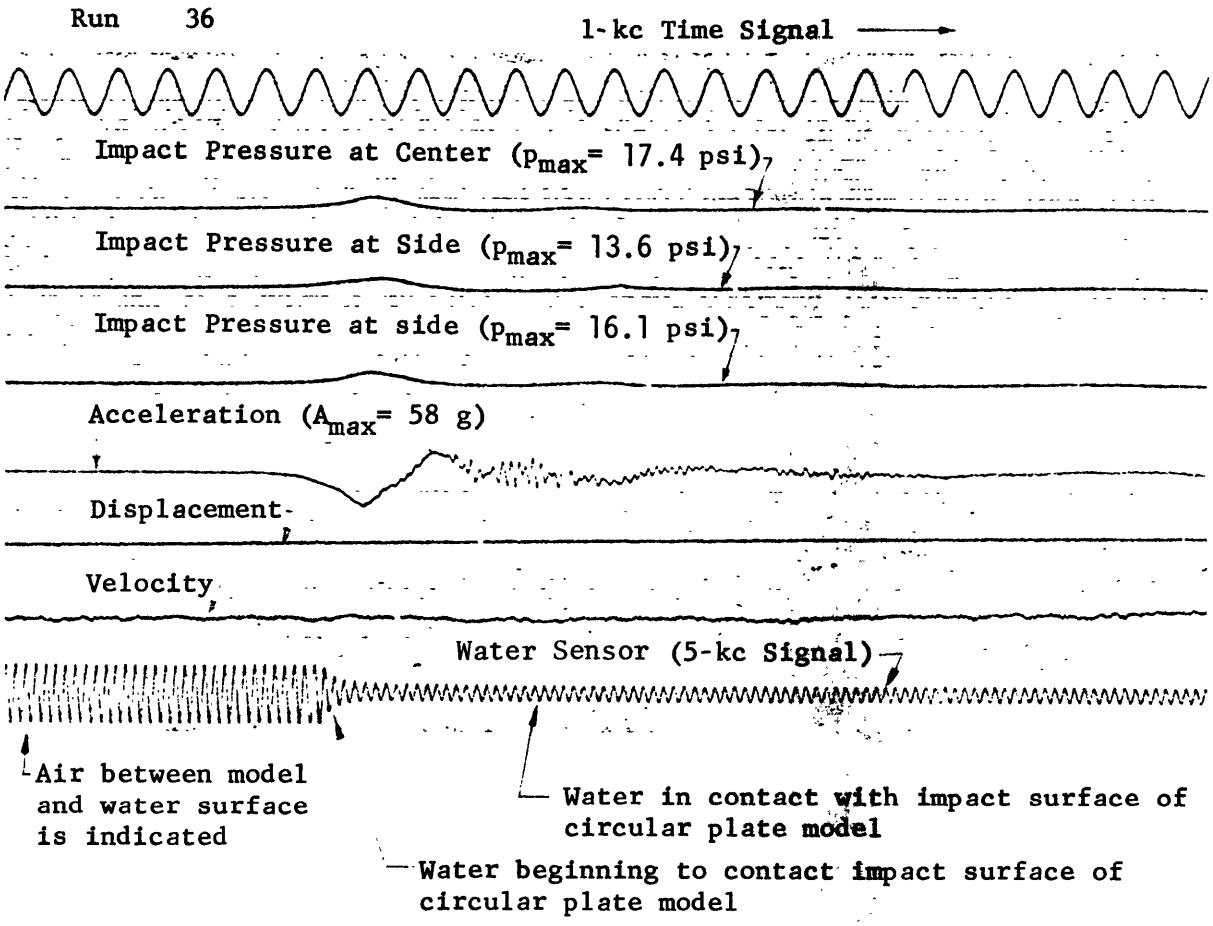

Figure 5 - Sample Record Showing Time Lag between Pulse of Maximum Impact Pressure and Escape of Trapped Air for Impact of Three-Dimensional Rigid Circular Plate

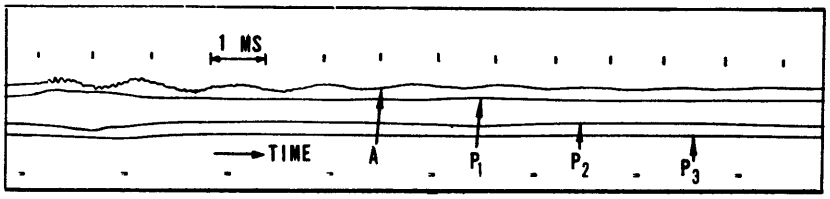

1-Deg Wedge

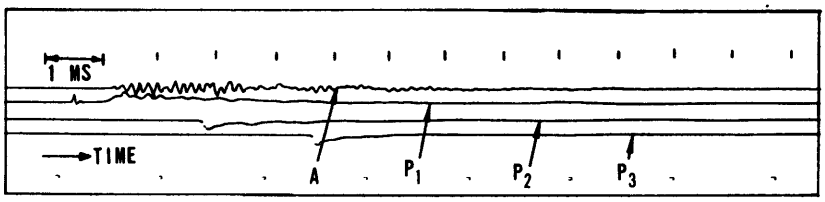

3-Deg Wedge

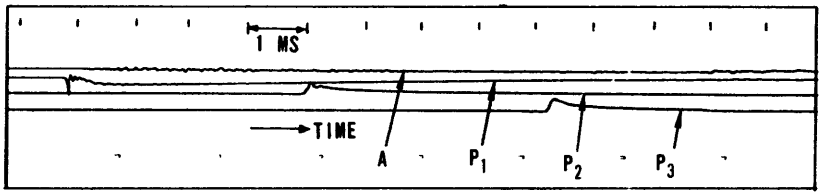

6-Deg Wedge

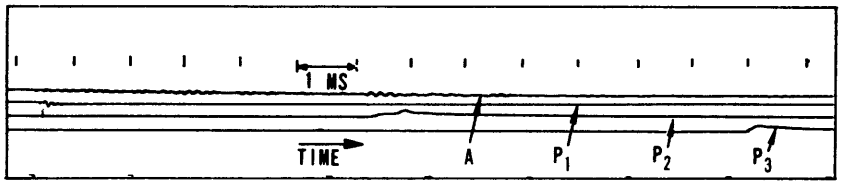

10-Deg Wedge

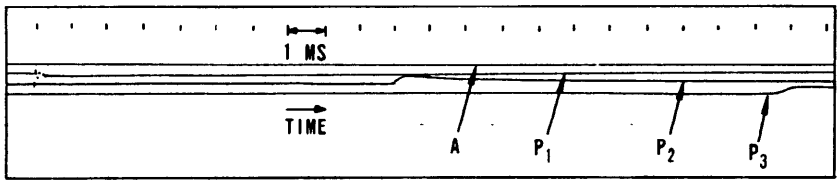

15-Deg Wedge

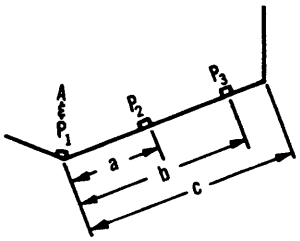

Gage Locations

MODEL DEADRISE ANGLE, DEG	1	3	6	10	15
RUN NUMBER	66-78	68-86	66-94	66-99	66-109
a X b X c, IN.	$3\frac{29}{32}$ X 7 $\frac{13}{16}$ X 10	$3\frac{29}{32}$ X 7 $\frac{13}{16}$ X 10	4 X 7 $\frac{29}{32}$ X 9 $\frac{31}{32}$	$3\frac{7}{8}$ X 7 $\frac{25}{32}$ X 10	$3\frac{31}{32}$ X 7 $\frac{27}{32}$ X 10 $\frac{1}{32}$
A - ACCELERATION AT KEEL, g	64 MAX	139 PEAK/PEAK	11 P/P	1.9 P/P	NIL
P_1 - MAXIMUM PRESSURE AT KEEL, PSI (IMPULSE/HYDRO)	0/33	15/11.2	15.3/5.5	28.5/3.8	23.4/2.8
P_2 - MAXIMUM PRESSURE a-IN. OFF KEEL, PSI	33	46	26.4	12.6	6.8
P_3 - MAXIMUM PRESSURE b-IN. OFF KEEL, PSI	20	48	25	11.8	5.5

Figure 6 - Sample Records Taken during 6-Inch Drop Tests of Rigid Wedge-Shaped Models

Figure 7 - Sample Records Taken during 6-Inch Drop Tests of Rigid Cone-Shaped Models

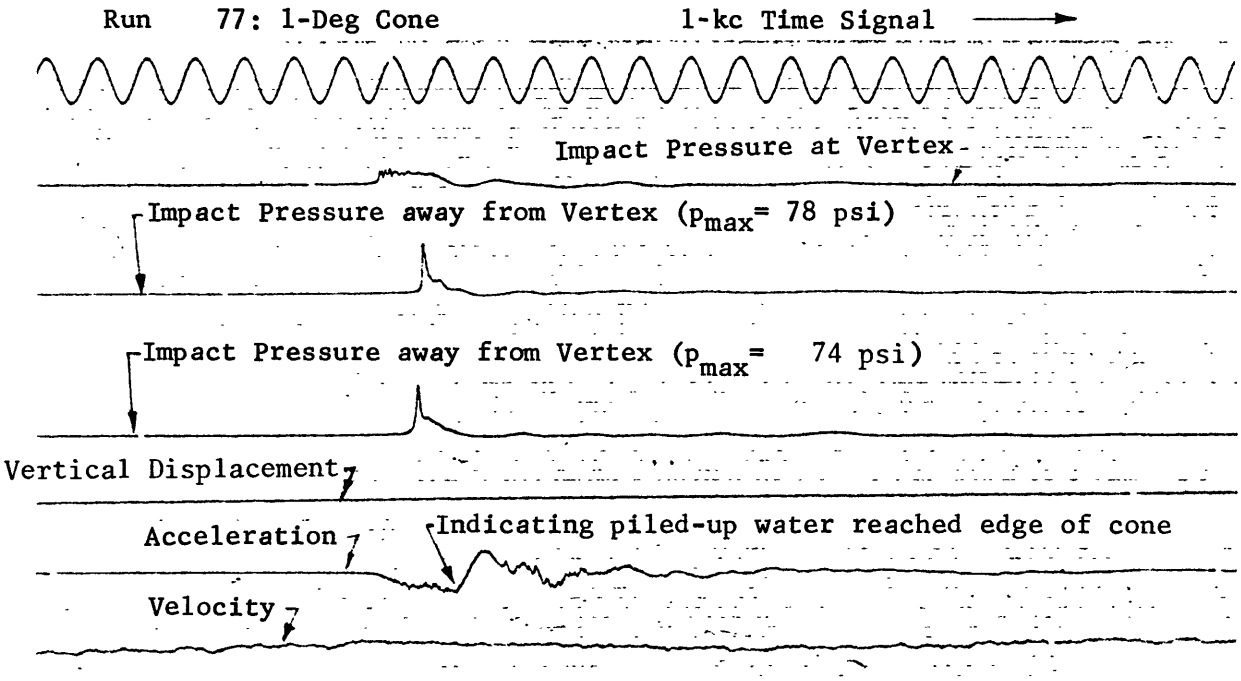

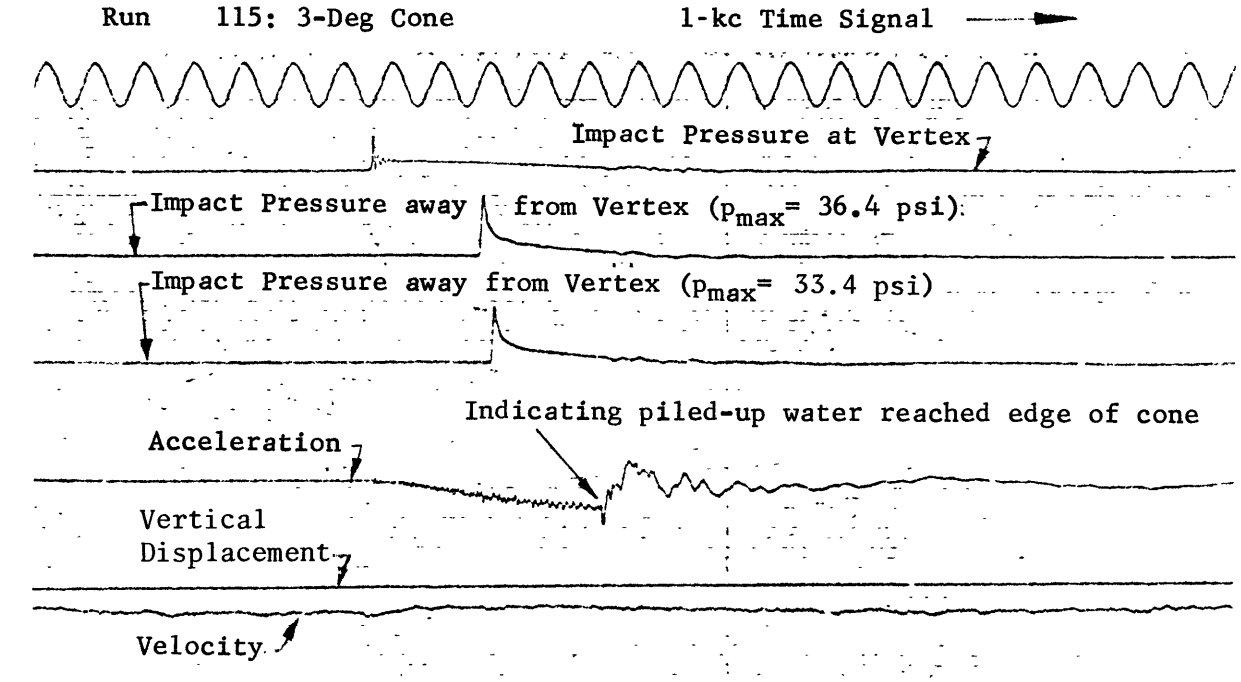

Figure 7 (Continued)

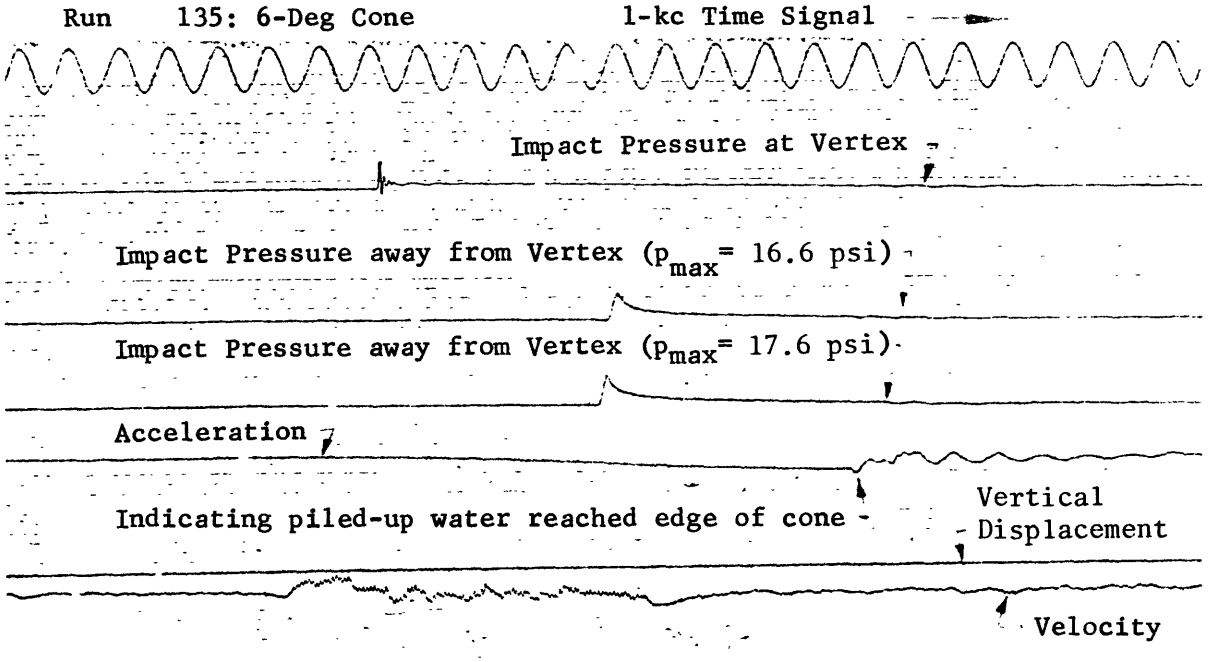

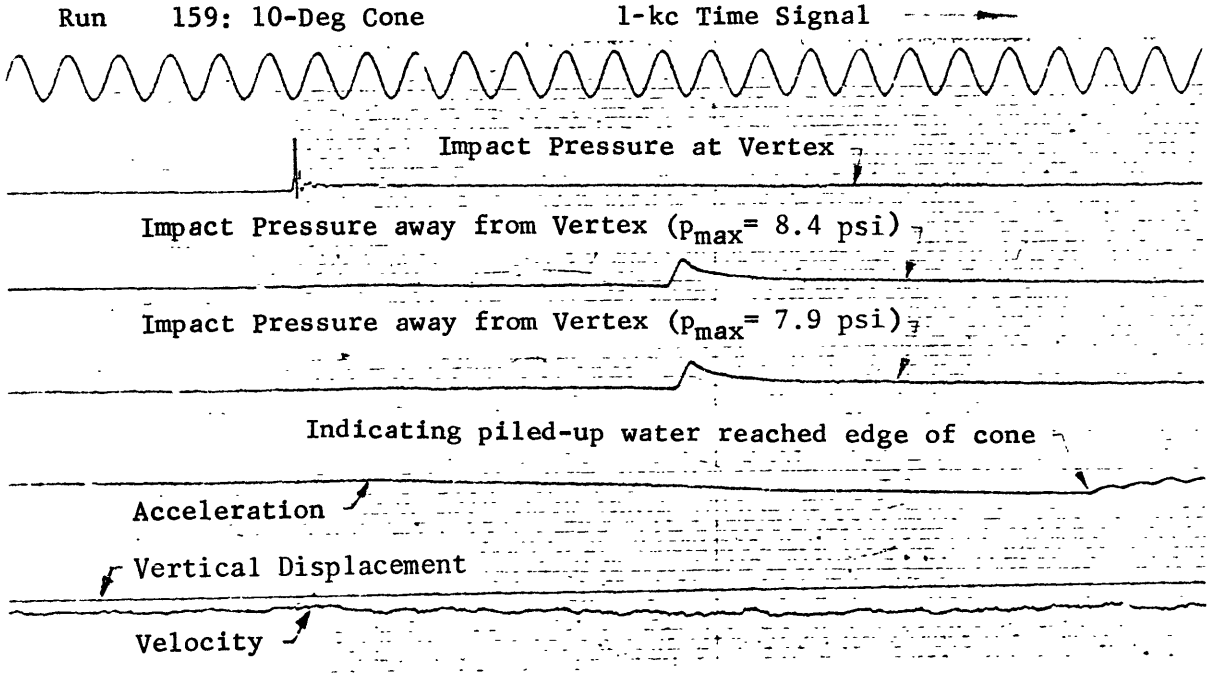

Figure 7 (Continued)

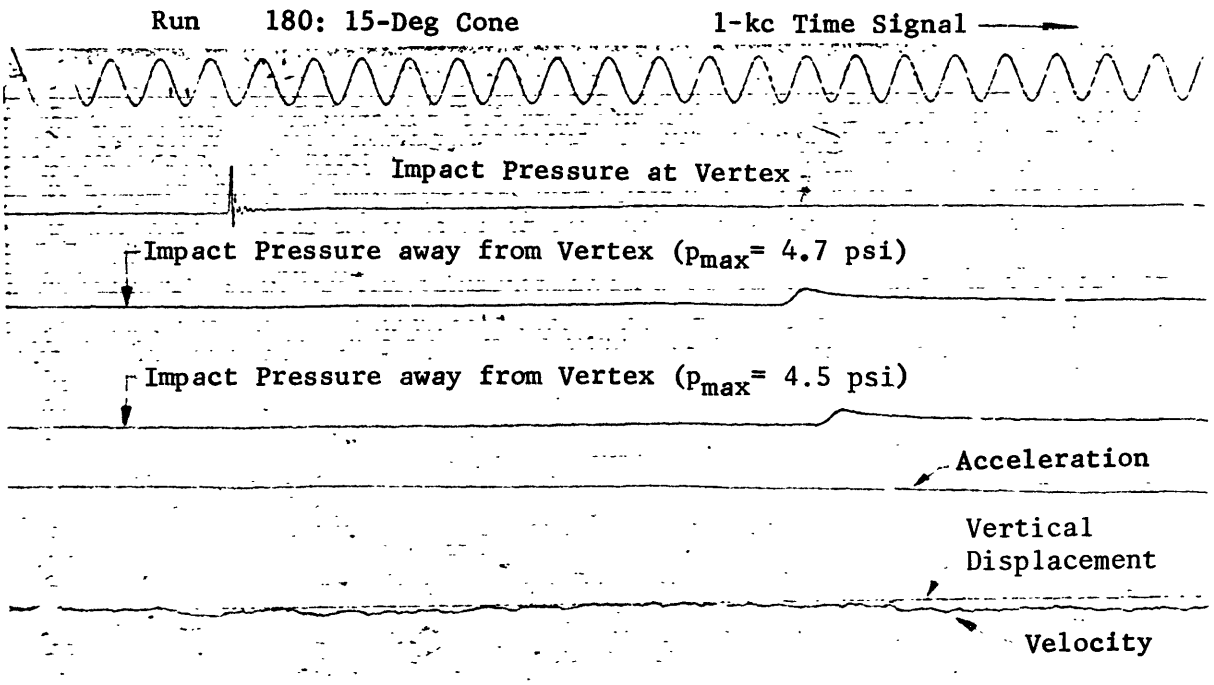

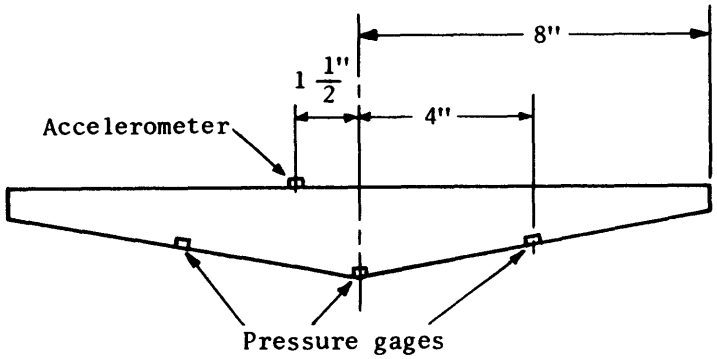

Gage Locations

Figure 8 - Experimental Results of Maximum Impact Pressure Caused by Water Impact of Rigid Wedge-Shaped Models

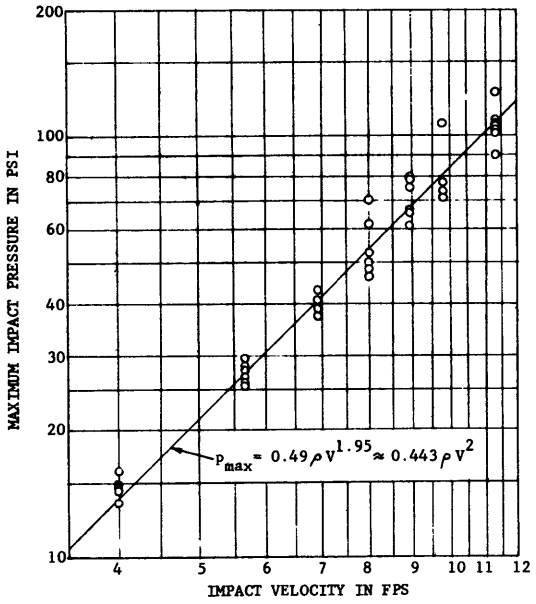

Figure 8a - Measured at Center of Flat-Bottom Model

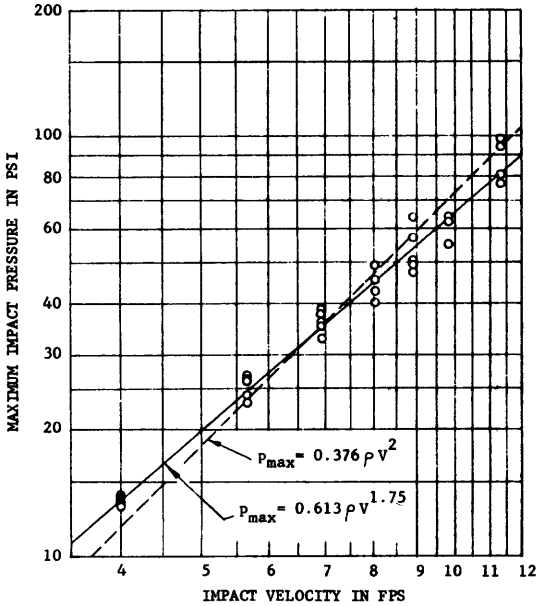

Figure 8b - Measured 6 11/16 Inches Off Center of Flat-Bottom Model

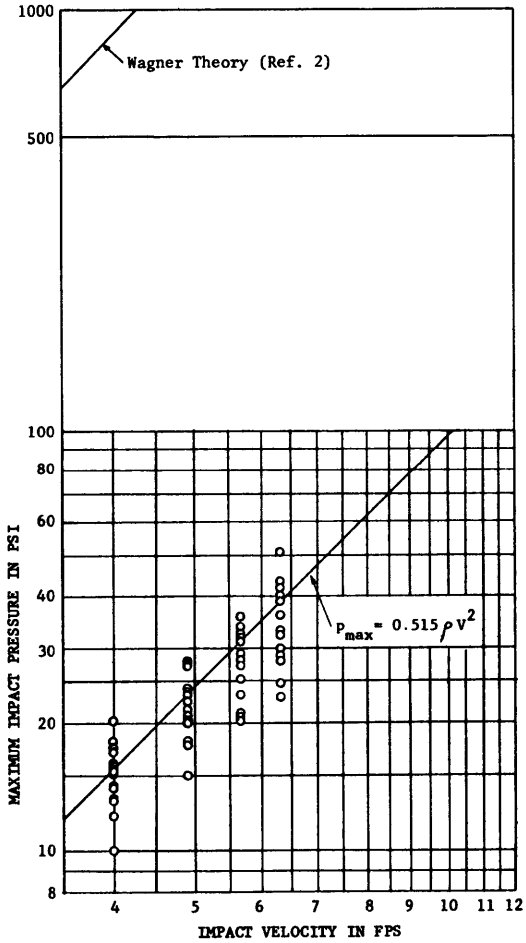

Figure 8c - Wedge-Shaped Model with 1-Degree Deadrise Angle

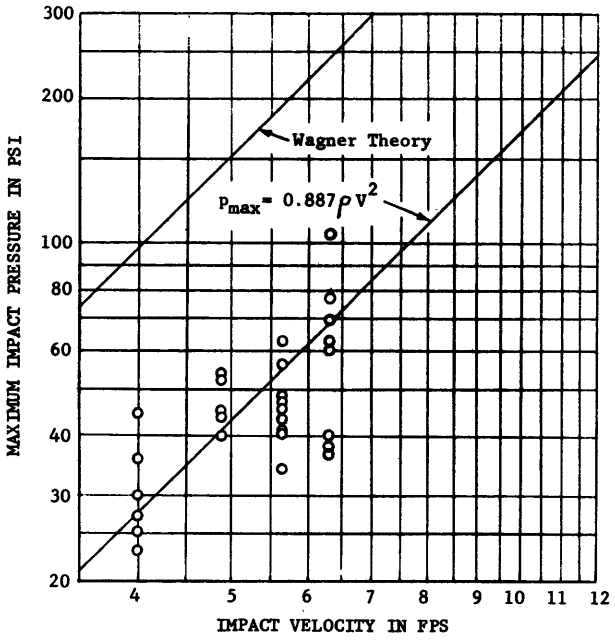

Figure 8d - Wedge-Shaped Model with 3-Degree Deadrise Angle

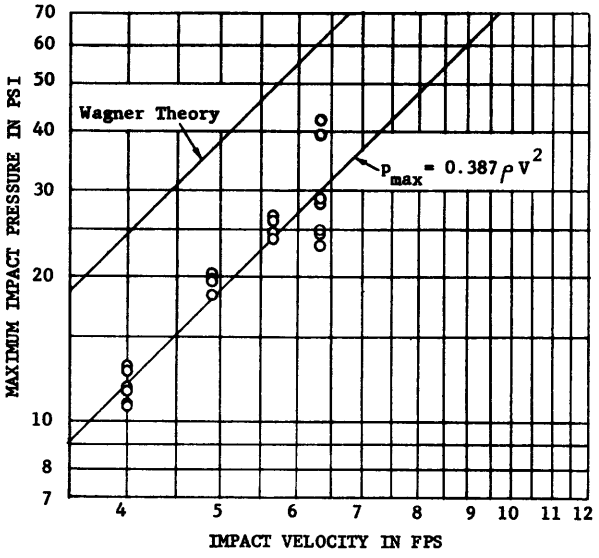

Figure 8e - Wedge-Shaped Model with 6-Degree Deadrise Angle

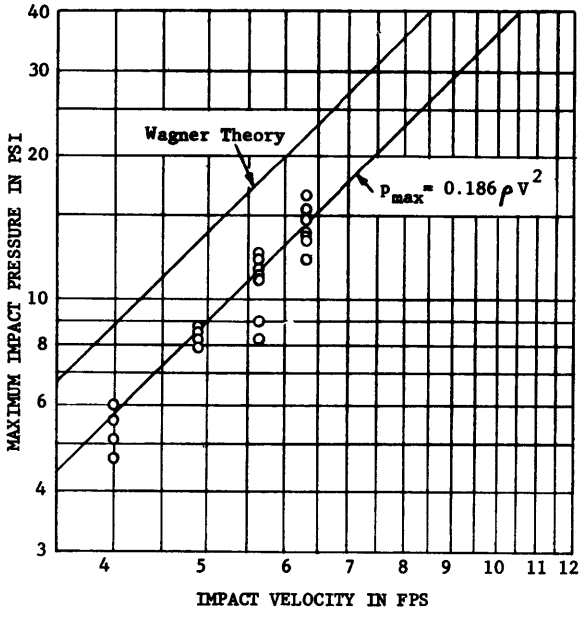

Figure 8f - Wedge-Shaped Model with 10-Degree Deadrise Angle

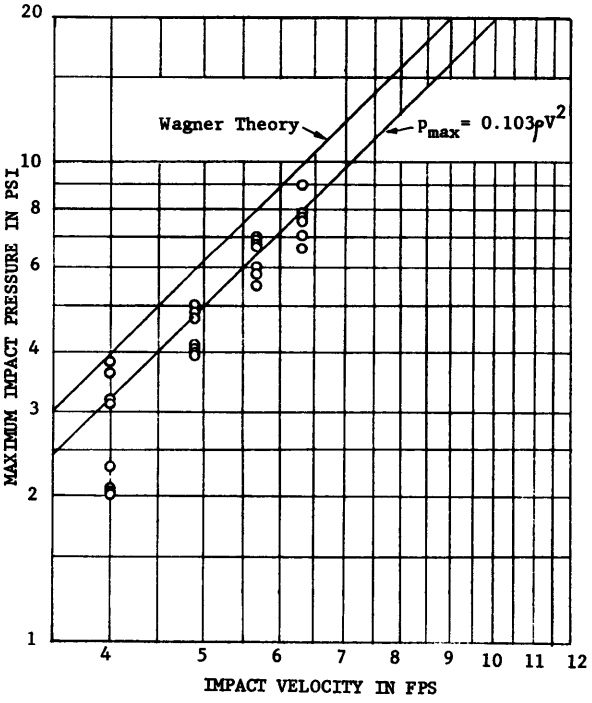

Figure 8g - Wedge-Shaped Model with 15-Degree Deadrise Angle

Figure 9 - Experimental Results of Maximum Impact Pressure Caused by Water Impact of Rigid Cone-Shaped Models

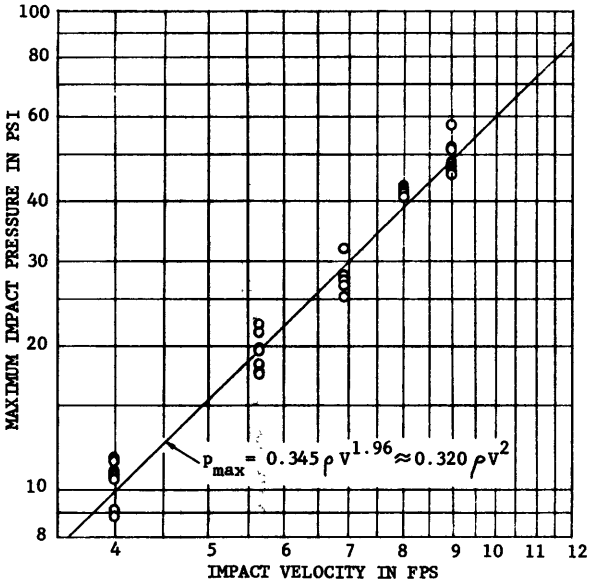

Figure 9a - Measured at Center of Circular Plate Model

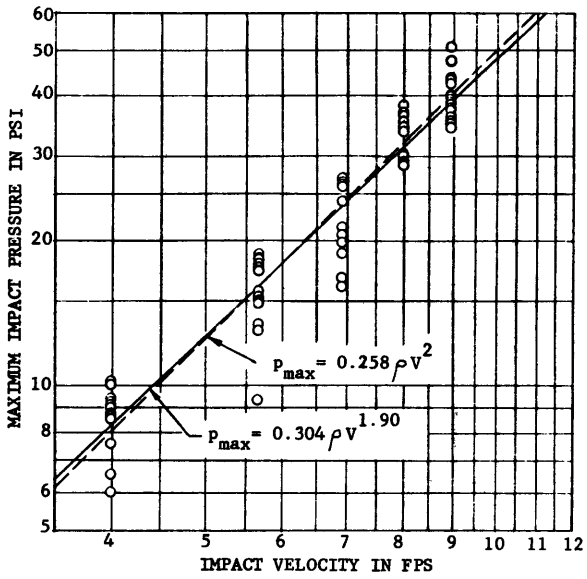

Figure 9b - Measured 4 Inches off Center of Circular Plate Model

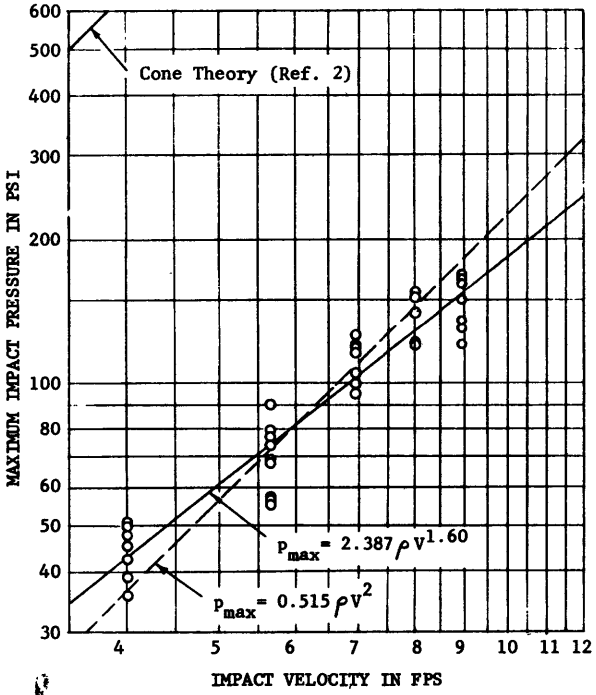

Figure 9c - Cone-Shaped Model with 1-Degree Deadrise Angle

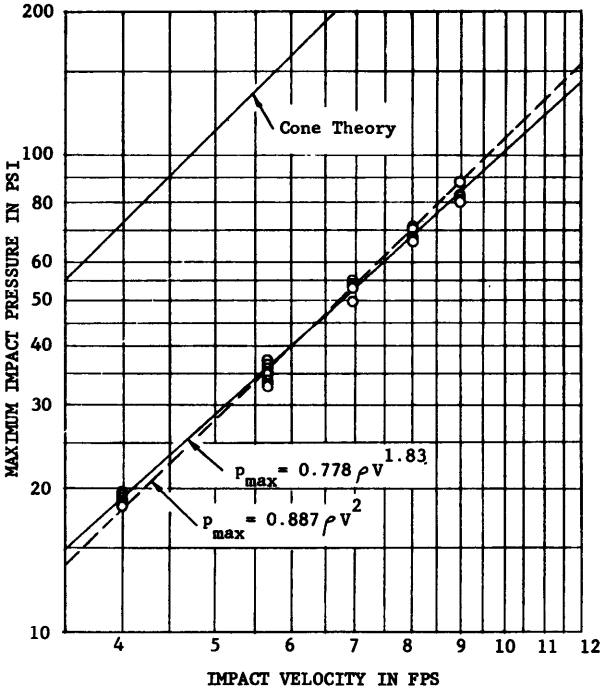

Figure 9d - Cone-Shaped Model with 3-Degree Deadrise Angle

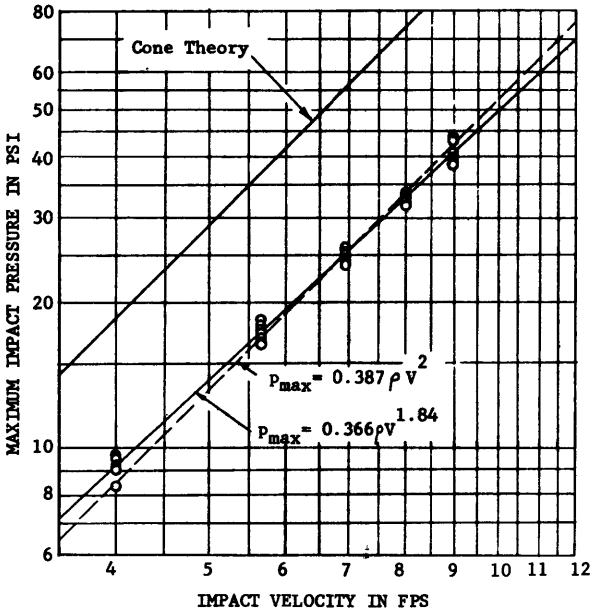

Figure 9e - Cone-Shaped Model with 6-Degree Deadrise Angle

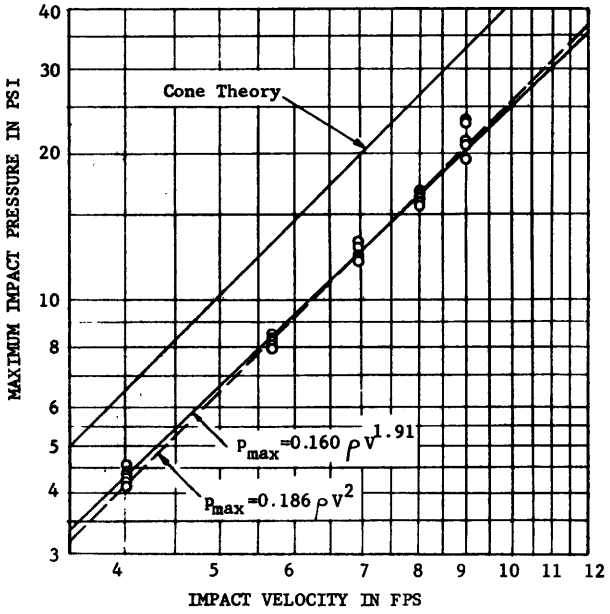

Figure 9f - Cone-Shaped Model with 10-Degree Deadrise Angle

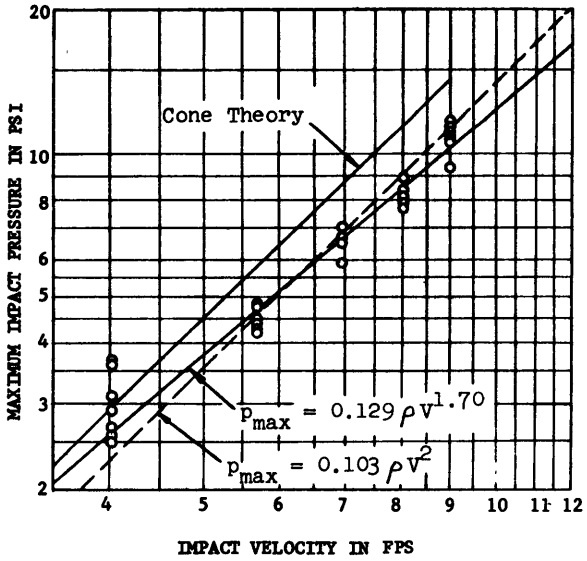

Figure 9g - Cone-Shaped Model with 15-Degree Deadrise Angle

APPENDIX A
INSTRUMENTATION

GENERAL DESCRIPTION

The general layout of the instrumentation array is shown in the functional block diagram of Figure A1.

The body force measuring channels consisted of three piezoelectric (PE) pressure gages, one linear PE accelerometer, and four identical charge amplifiers. The charge amplifier output voltage signals were amplified and recorded on Channels 2 through 5 of the magnetic tape recorder.

The vertical displacement, Channel 6, consisted of a linear potentiometrical displacement gage and a displacement box which included a constant-current gage drive and an amplifier to drive the tape recorder. This box also included a differentiator circuit for obtaining a vertical velocity signal which was recorded on Channel 7. A secondary calibration system referenced to the basic physical quantities of distance (in feet), time (in seconds) and velocity (in feet per second) was included in this same unit (labeled "displacement box" in Figure A1).

A water contact sensor, Channel 8, and a 1-kc sinusoidal timing reference, Channel 1, completed the eight-channel datum input to the Ampex CP-100 magnetic tape recorder.

A calibration switch box allowed a sequential electrostatic charge calibration of the PE body force measuring channels before the model was released. This unit also activated the drop solenoid which released the model at the end of the sequential charge calibration.

The data were recorded at 60 IPS and played back at the end of the run at 1 7/8 ips onto a 7-in. CEC oscillograph for immediate on-the-spot inspection and analysis.

GENERAL FEATURES OF CIRCUIT DESIGNS

Displacement and Velocity Measurement System

The displacement and velocity measurement system is illustrated in the systemic block diagram of Figure A2. The general features of the circuit designs of each systemic section are described. The theoretical aspects will be discussed in a later section.

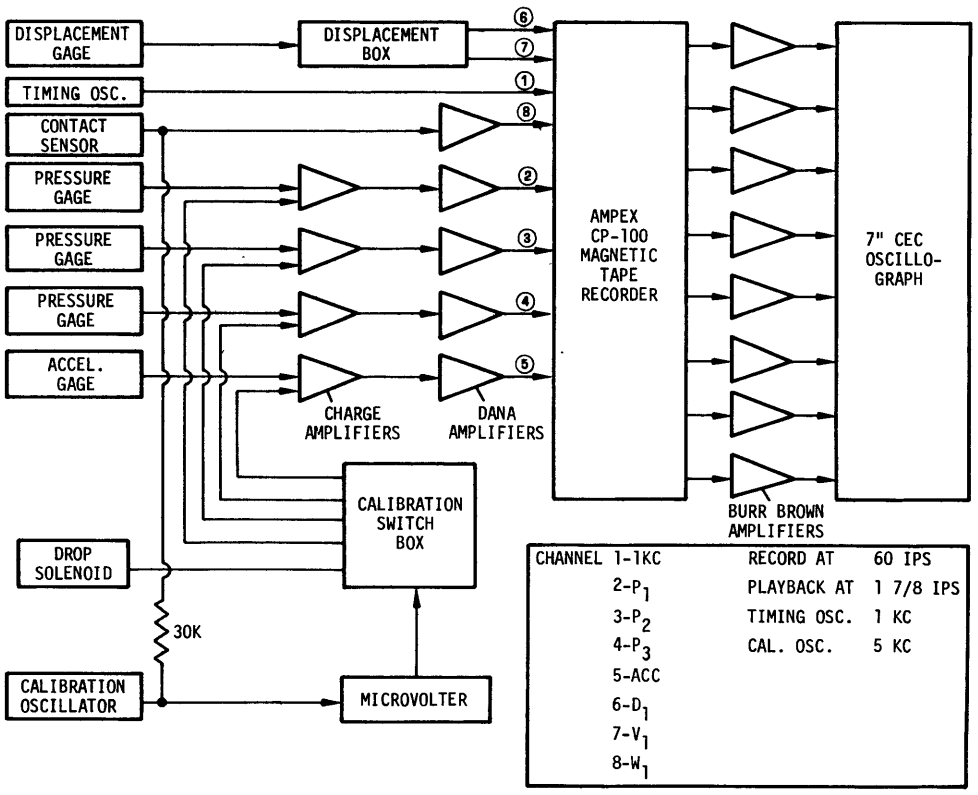

Figure A1 - General Layout of Instrumentation Array

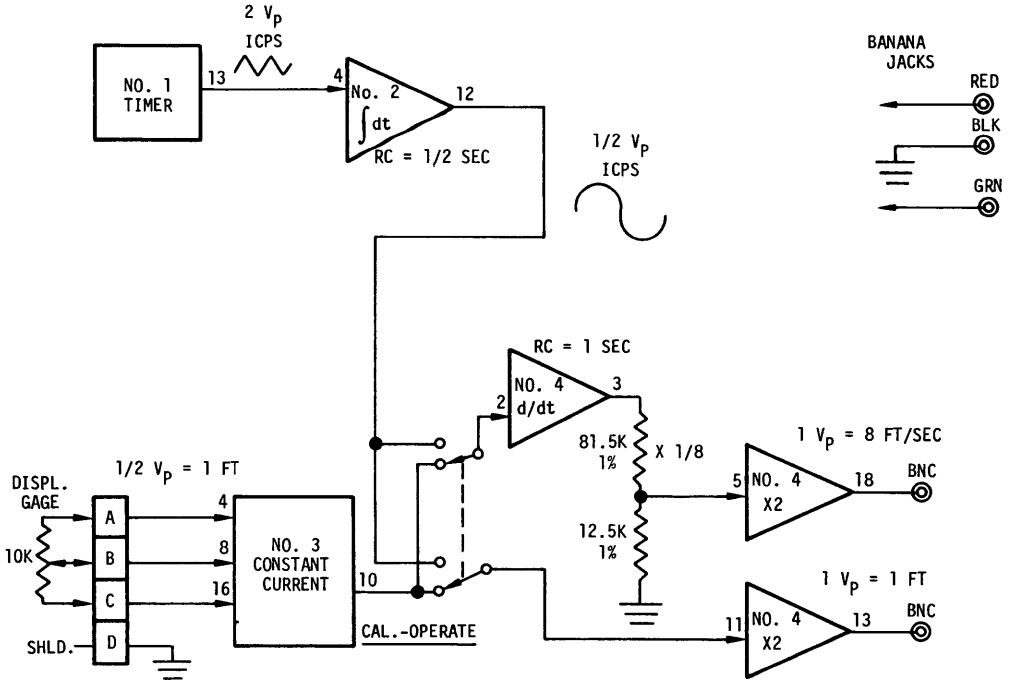

Figure A2 - Displacement and Velocity Measurement System

Displacement Potentiometrical Transducer: The vertical displacement measurement transducer consisted of a 10K-ohm, 10-turn potentiometer.* The body of this transducer was affixed to the stationary frame of the "drop" apparatus. Mounted on the shaft potentiometer was a sheave pulley with serrations to receive a light beaded chain that connected to the model. The beaded chain passed up over this pulley and was tensioned by means of a small lead weight.

As shown in Figure A3, two field effect transistors (FET) were connected in series with a 2.5K-ohm resistor which shunted the displacement potentiometer. The lower FET served as a constant-current (cc) generator to energize the transducer. The 1K-ohm rheostat in this cc circuit was adjusted so that when the beaded chain was moved exactly 1 ft (thus rotating the shaft of the potentiometer), the resultant voltage change on the slider was precisely 0.5v. The upper FET circuit was adjusted so that with the model just touching the water surface, the voltage on the slider was precisely zero. The operational follower amplifier provided the low impedance required to drive the differentiator circuit in the displacement velocity converter.

Calibration Signal Generator: The circuitry for the calibration signal generator is shown schematically in Figure A4. A high-gain operational comparator (741C on left side) was coupled by a resistance train to an operational integrator (741C center). The comparator abruptly changed state when its two input terminals (Terminals 4 and 5) were equal. A square wave with an amplitude of 14 VP was integrated to provide a symmetrical triangle at Terminal 10 of the integrator (741C center). The amplitude of this triangular wave was about 6 VP. This amplitude was trimmed to precisely 2 VP by the 10K-ohm potentiometer shown. A unit-gain follower (741C right side) provided low-impedance isolation. The timing period was precisely 1 sec, $\pm \frac{1}{3000}$ sec. Trimming adjustment is provided

---

*K = 10^3 ohm.

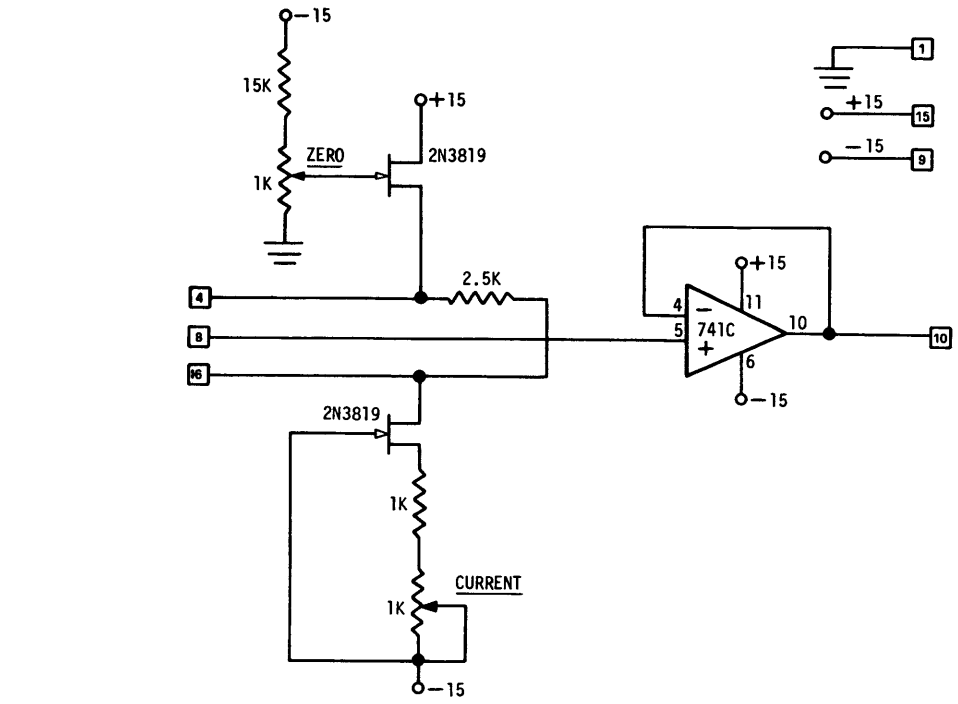

Figure A3 - Constant Current Circuitry for Energizing the Displacement Potentiometrical Transducer

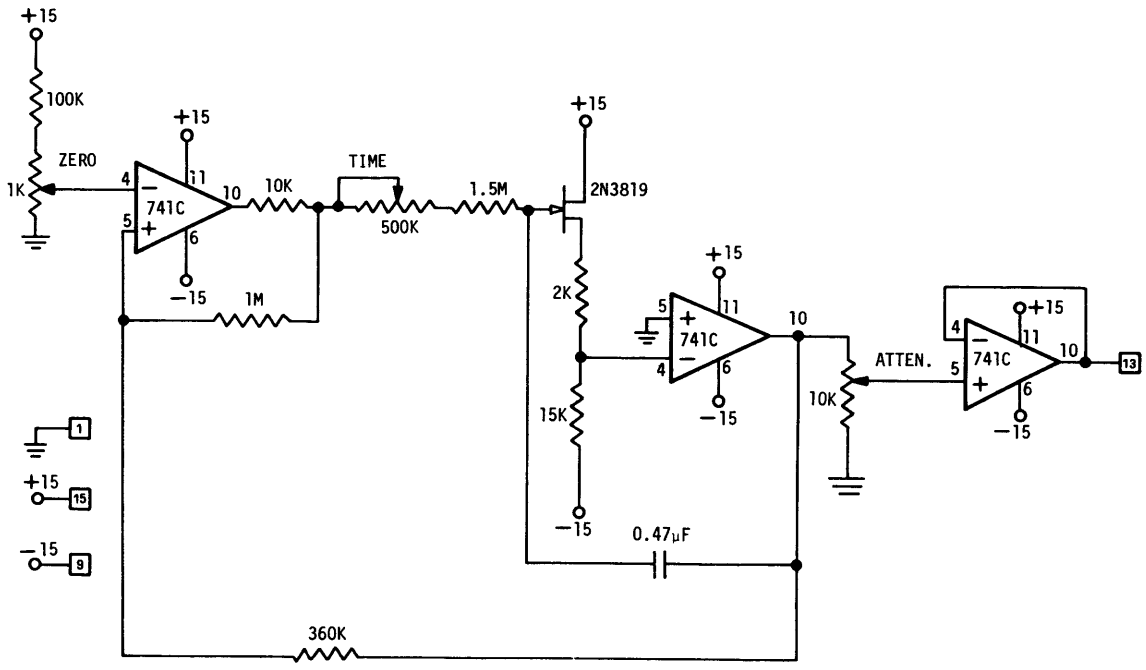

Figure A4 - Displacement and Velocity Calibration Signal Generator

by the 500K-ohm potentiometer in the resistance train. The zero line and amplitude stability of this total circuit were excellent, being in the order of a part in 5000 or better.

Output Card Tab 13 led to Input Card Tab 4 on the parabolic wave generator shown in Figure A5.

Parabolic Wave Generator: The parabolic wave generator is shown schematically in Figure A5. This unit is best described as a highly sophisticated operational integrator. The integrator proper is shown on the left side of the illustration. The right-hand circuitry was a high-accuracy zero-line stabilizer which constituted the principal difference between this and conventional operational integrating circuits. The two RC networks (3.3M/.047 μf, 330K/.47 μf)* acted as a negative feedback absorption filter, which removed the dynamic output from the integrator. The zero-line or d-c component passed without attenuation through the right hand 741C amplifier which had a gain of times 10. The "clean" output of this amplifier was fed to positive input Terminal 5 of the integrator. This became 100 percent "negative" feedback because of the phase reversal in the X10 amplifier. The resultant stability factor for the zero-line was about one part in 50,000.

Displacement Velocity Converter: The displacement velocity converter consisted of a conventional operational differentiator shown schematically at the upper left side of Figure A6. The displacement signal entered on Card Tab 2. The sensitivity of the converter had a fine adjustment control, the 1M-ohm potentiometer shown. This control was adjusted as follows. The parabolic wave train with an amplitude of 0.5 VP was imposed on Card Tab 2. This represented a displacement of 1 ft. At Terminal 10 of the 741C (upper left) differentiator, the issue had to be a triangular wave train with a period of precisely 1 sec and an amplitude of 4 VP. This represented a velocity of 8 fps. In other words, the

---

*M = 10^6 ohms and μf = 10^{-6} farad.

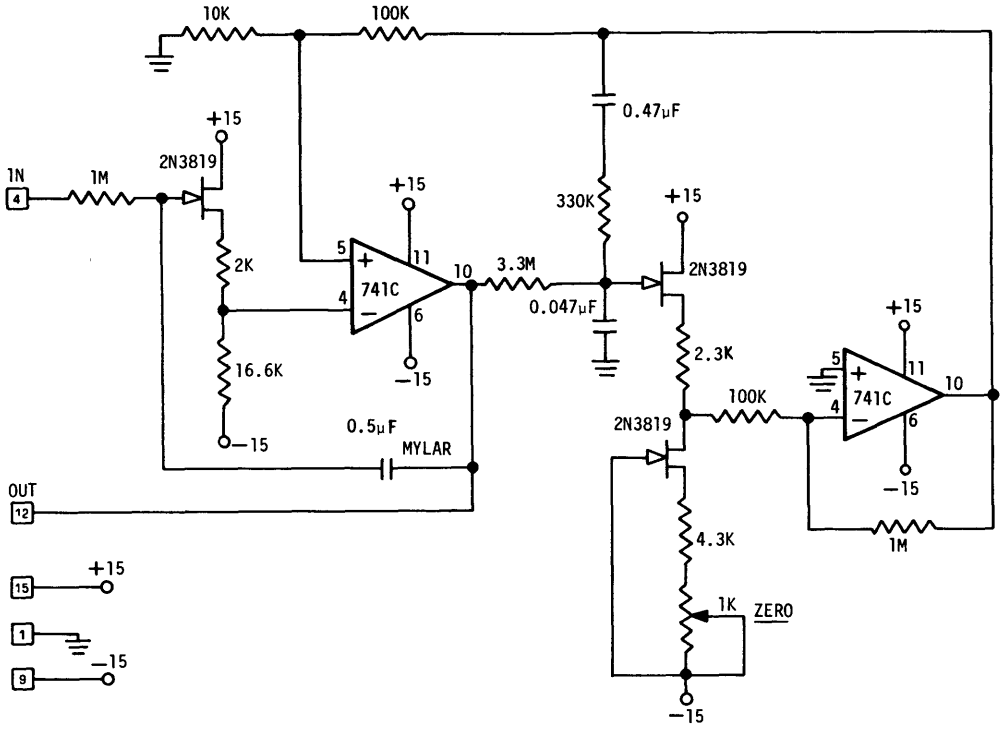

Figure A5 - Parabolic Displacement Wave Generator

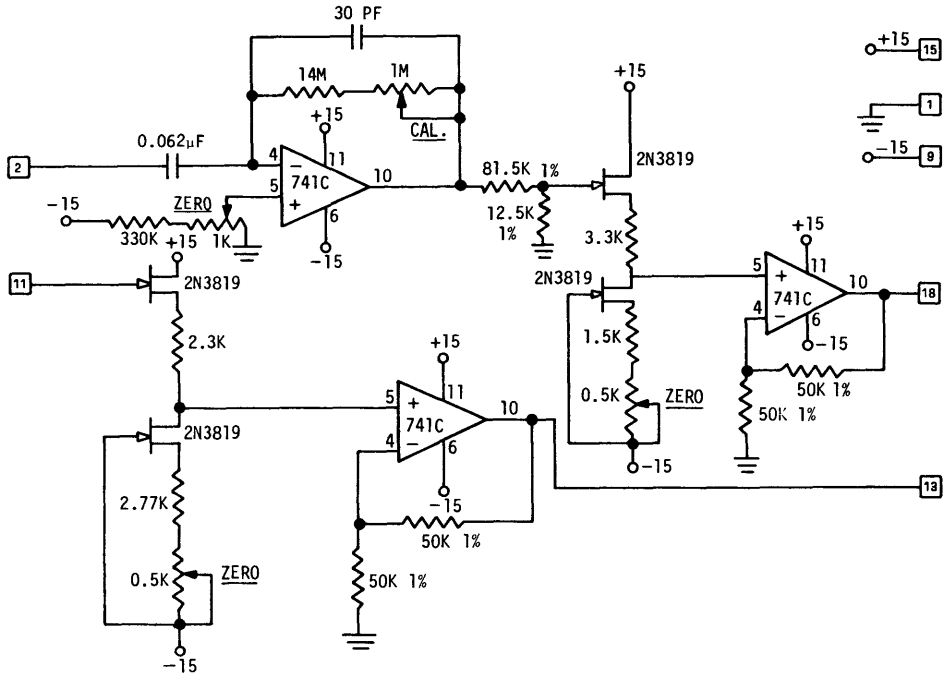

Figure A6 - Displacement Velocity Converter

triangular output wave from the differentiator had to be twice the exact replica of the 2-VP triangular wave that was impressed on the parabolic wave generator. The factor of two results from the practical requirement of a 1/2 sec time constant in the parabolic wave generator. This replication was the heart of the accuracy of the entire velocity system. After this fine adjustment was completed, the true displacement signal from the potentiometrical transducer (which had been calibrated to yield 0.5 VP/ft) could be switched through this same differentiator circuitry and thus read out true velocity.

In order to fit the amplitude scale of the tape recorder, the 4-VP triangular wave was passed through the 1/8-attenuator, thence through the x2 operational amplifier on the right side. Now 1 VP corresponded to a velocity of 8 fps. The lower x2 operational amplifier served to convert the 1/2 VP displacement signal to 1 VP or 1v per foot of model travel.

Water Contact Sensor

The water contact sensor was designed to indicate the exact instant that the model touched the water surface. As shown in Figure A1, a 30K-ohm resistor was connected to the 5-kc calibration oscillator. Two small foil plates were attached on the bottom of the model; these were centrally located but insulated. One plate connected to the 30K-ohm resistor and also went to an amplifier for recording on "mag" tape. The other plate connected to the signal ground. When the water was contacted, these two plates were thereby essentially short-circuited and the amplitude of the 5 kc wave train was reduced to approximately one-tenth. This provided a simple but effective indication of the time of contact with the water.

CALIBRATION TECHNIQUES

Body Force Calibration

The body force measuring transducers consisted of three PE pressure gages and one linear PE accelerometer. Four identical charge amplifiers were utilized to electronically convert the charge signals to voltage signals for amplification and recording.

Because a PE transducer inherently issues a charge (q) signal rather than a voltage (v) signal, a basic charge calibration rather than a voltage calibration was used to calibrate the entire system. This calibration was based on the basic relationship (Coulomb's Law):

$$Q = CV$$

The charge calibration signal was generated by using the 5-kc oscillator shown in Figure A1 and driving this voltage into the calibration input of the respective charge amplifiers. The calibration inputs consisted of 100-pf capacitors* between the calibration and signal inputs of the amplifier. Thus a charge calibration signal (q) was generated which was the combination of the 5-kc oscillator (voltage v) and the 100-pf capacitor (capacitance c).

The amplitude, and thus the peak value, of this charge calibration signal was adjusted precisely by the microvolter shown. The sensitivities of the individual PE gages were given either in 10^{-12} coulombs per pound-per-square-inch or per g. Now a known calibration of the approximate unit of measure peak-to-peak could be impressed on each respective channel. An illustration of this conversion of units is presented below.**

$$\frac{\text{charge calibration signal (pcb P-P)}}{\text{gage sensitivity (pcb/psi)}} \equiv \text{calibration value (psi P-P)}$$

where

$$\text{gage sensitivity} = X \text{ pcb/psi}$$

$$C = 100 \text{ pf}$$

$$v = \frac{NX}{2\sqrt{2}} \text{ v rms}$$

$$1 \text{ v rms} = 2\sqrt{2} \text{ v (P-P)}$$

---

*pf = 10^{-12} farad.

**pcb P-P = 10^{-12} coulombs peak to peak.

$$\underbrace{\frac{\frac{NX}{2\sqrt{2}}\ v\ rms}{1} \times \frac{2\sqrt{2}\ v\ (P\text{-}P)}{1\ v\ rms} \times \frac{100\ pf}{1}}_{q\ (cal)} \times \underbrace{\frac{psi}{x\ pcb}}_{\substack{gage \\ sensitivity}} = \underbrace{100N\ psi}_{\substack{desired\ cal \\ value}}$$

Theoretical Aspects of the Free-Fall Calibration

The free-fall calibration system was of the secondary type. It automatically produced analog voltages that were referenced to the basic physical units of distance (in feet) time (in seconds), and velocity (in feet per second). The method permitted on-record comparison between the actual motion of a dropped body and the electronically simulated motion of a body in free fall under ideal conditions.

A functional wave generator (TIMER 1 in Figure A2) delivered a triangular wave train which was accurately symmetrical about its zero line and which had a periodicity of precisely 1 sec. This wave train had a single peak amplitude of 2v, or 2 VP.

The triangular wave train is impressed on an operational integrator (Item 2). The issue from the integrator is a symmetrical parabolic wave train also with a periodicity of precisely 1 sec and having a single peak amplitude of 0.5v or 0.5 VP.

With the CAL-OPERATE switch in the CAL position, the parabolic wave train was impressed on an operational differentiator (Item 4 (d/dt) on Figure A2). The issue from the differentiator was a replica of the original triangular wave train with an amplitude of 4 VP. After passing through a fixed attenuator (x 1/8) and an amplifier (x2), the triangular wave train had an amplitude of 1 VP which represented and corresponded to a linear velocity wave train with a single peak amplitude of 8 fps.

Simultaneously, the parabolic wave train passed through another amplifier (x2) and issued with an amplitude of 1 VP which represented and corresponded to a free-fall displacement wave of 1 ft.

The significance and meaning of this parabolic wave train requires some discussion. The physical situation being electronically simulated was that of an imaginary acceleration field with an acceleration force of

1 g continuously directed toward a line or plane. Thus if an object is held 1 ft from this plane and then dropped, it will fall under a constant accelerating force g until it passes through the plane. At this instant, the force encountered is exactly reversed, whereupon the velocity decreases to zero, the object "falls" back through the plane, and in 1 sec again reaches the position from which it was initially dropped. In the assumed absence of frictional or any other forces, the object follows this parabolic displacement pattern indefinitely.

The accelerating force acting on the object just described is shown in Figure A7a as a symmetrical square wave. Figure A7b depicts the velocity pattern which, of course, is a symmetrical triangular wave. Figure A7c presents the displacement pattern which is the parabolic wave train under discussion.

A single parabolic arch of this displacement wave train is shown in Figure A8. The concept represented by this illustration is as follows: an object with a velocity of 8 fps directed upward along OH emerges at the origin 0. This object continues to travel upward at decreasing velocity until the height H is reached, at which point its velocity is zero. Immediately thereafter, the body falls from H through the origin 0 at a velocity which increases linearly with time.

The parabolic arch or curve is a true time-history of the displacement of the body from the time of its emergence at the original 0 until it falls through the same point on exit. This curve serves to spread the motion on a convenient time scale to show the detail of the solely vertical excursion. There is no horizontal motion, and none should be inferred.

The classical formulation for a parabola of this type and kind is:

$$x^2 = 2\,py$$

where p is the sizing parameter (i.e., P/2 is the distance from the focus to the vertex) and 2p spans the width of the curve in a sector cut through the focus.

Since the displacement s of a falling body is described by the expression:

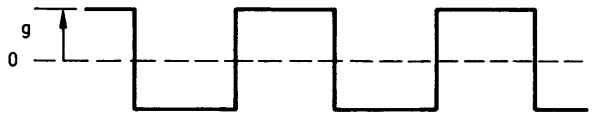

Figure A7a - Acceleration Wave Train $\frac{4g}{\pi}\sum_{n=0}^{\infty}\frac{\cos n\omega t}{n}\sin\frac{n\pi}{2}$

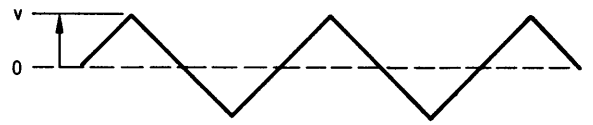

Figure A7b - Velocity Wave Train $\frac{8v}{\pi^2}\sum_{n=0}^{\infty}\frac{\sin n\omega t}{n^2}\sin\frac{n\pi}{2}$

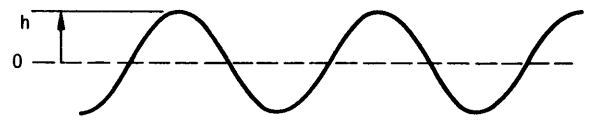

Figure A7c - Displacement Wave Train $\frac{32h}{\pi^3}\sum_{n=0}^{\infty}\frac{-\cos n\omega t}{n^3}\sin\frac{n\pi}{2}$

Figure A7 - Illustrations and Fourier Series Representations of Acceleration (Square), Velocity (Triangular), and Displacement (Parabolic) Wave Trains

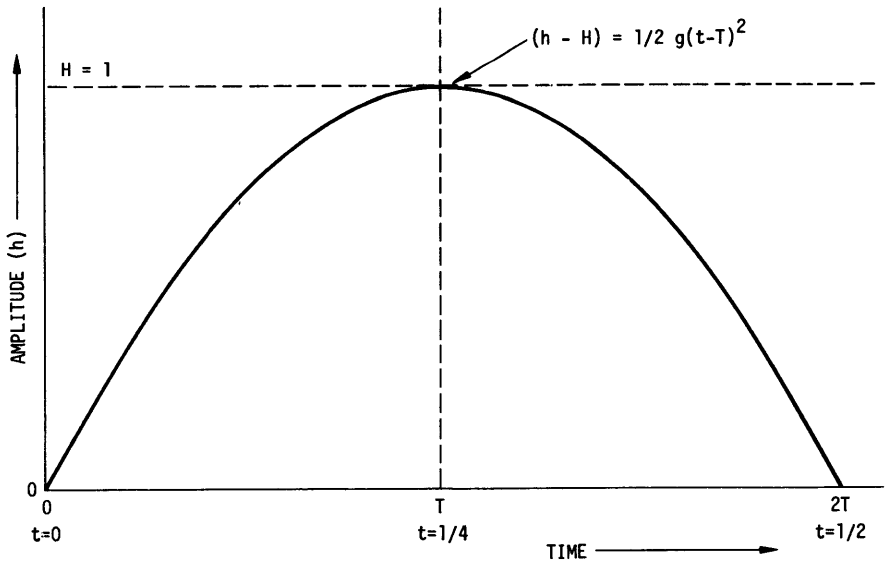

Figure A8 - Single Parabolic Arch of the Displacement Wave Train

$$s = 1/2\ gt^2$$

the classical formulation is modified by adjusting the nomenclature and by moving the origin 0 to the left-hand side as shown in the illustration. This modification and translation is accomplished as follows:

Step 1. Let $x = t$, $y = h$, and $p = -1/g$. Then

$$t^2 = (-2/g)h$$

Step 2. Move origin 0 to (-T, -H). Then

$$(t - T)^2 = (-2/g)\ (h-H)$$

where h is the instantaneous height above the origin 0,
H is the maximal height of h,
t is the instantaneous time notation, and
T is the particular value of t at midpoint under the vertex.

Step 3. Set limits $0 \leq t \leq 2T$. Then

$$(t - T)^2 \lim_{t = 0 \to 2T} = (-2/g)\ (h-H)$$

and for this particular calibration system: H = 1 ft, g = 32 ft/sec,^{2} and T = 1/4 sec. Then

$$(t - 1/4)^2 \lim_{t = 0 \to 1/2} = -\frac{1}{16}\ (h-1)$$

OPERATIONAL PROCEDURES

The system was connected as shown in the general layout of the instrumentation array, Figure A1. Calibration and gain setting values for the various model shapes and drop height conditions were preset. These values were readjusted or updated as experience warranted prior to each run or drop. The potentiometrical transducer was adjusted so that at the water level it read precisely zero on the DVM provided for this purpose. The model was then elevated to the desired drop height and suspended by the drop solenoid. The Ampex CP-100 magnetic tape recorder was set up to record at 60 ips.

With these initial setup conditions met and the proper warmup conditions for each systemic unit satisfied, the following steps have to be performed in sequence:

1. Turn the displacement box switch to the CAL position.
2. Turn the tape recorder to RECORD.
3. After approximately 5 sec, turn the displacement box back to the OPERATE position.
4. Next, slowly rotate the drop switch on the calibration switch box from Position 1 to Position 7 - this sequentially calibrates the PE gage channels and then releases the model.
5. Approximately 5 sec after the model drops, stop the tape recorder.
6. Rotate the drop switch on the calibration switch box back to Position 1.
7. Turn the displacement box switch back to the CAL position.
8. Rewind the tape and playback at 1 7/8 in/sec on the 7 in. CEC oscillograph.
9. Analyze the record and adjust gain settings and CAL values as required for the next run.

APPENDIX B

A FORTRAN IV PROGRAM TO FIT TEST DATA BY THE METHOD OF LEAST SQUARES

Assume that the test data points can be fitted with the equation

$$p = k\, V^n$$

which may be rewritten as

$$\log p = \log k + n \log V$$

This equation is a form of

$$Y = a_o + a_1 X$$

If there are N numbers of test data points, then by the method of least squares,

$$\sum_1^N Y_N = a_o N + a_1 \sum_1^N X_N$$

$$\sum_1^N X_N Y_N = a_o \sum_1^N X_N + a_1 \sum_1^N X_N^2$$

These two equations give

$$a_o = \frac{\sum_1^N Y_N \sum_1^N X_N^2 - \sum_1^N X_N \sum_1^N X_N Y_N}{N \sum_1^N X_N^2 - \left[\sum_1^N X_N\right]^2}$$

$$a_1 = \frac{N \sum_1^N X_N Y_N - \sum_1^N X_N \sum_1^N Y_N}{N \sum_1^N X_N^2 - \left[\sum_1^N X_N\right]^2}$$

Thus

$$n = a_1$$

$$k = \log^{-1} a_o$$

If the test data points are forced to fit into the equation

$$p = k V^2$$

For N numbers of test data points,

$$k = \frac{\sum_1^N k_N}{N} = \frac{\sum_1^N (P_N/V_N^2)}{N}$$

The computer program for this simple mathematical operation is as follows:

```
 10  DIMENSIØN X(100),Y(100),P(100),V(100),Z(100)
 12  READ,NCASES
 15  DØ 50 NC=1,NCASES
 20  READ,N
 30  DØ 10 I=1,N
 40  10 READ,P(I),V(I)
 50  XN=N
 60  DØ 20 I=1,N
 70  Y(I)=ALØG (P(I))
```

```
 80  X(I)=ALØG (V(I))
 85  20 Z(I)=V(I)*V(I)
 90  B=0.0
100  C=0.0
110  D=0.0
120  E=0.0
130  F=0.0
135  AJ=0.0
140  DØ 30 I=1,N
150  B=B+X(I)
160  C=C+Y(I)
170  D=D+X(I)*Y(I)
180  E=E+X(I)*X(I)
185  30 AJ=AJ+P(I)/Z(I)
190  F=B*B
200  G=XN*E-F
210  AØ=(C*E-B*D)/G
220  AØ=EXP(AØ)
230  AI=(XN*D-B*C)/G
235  AK=AJ/XN
240  PRINT 40 AØ,AI,AK
250  40 FØRMAT(5X,6H AØ = ,F7.5,5X,6H AI = ,F7.5,5X,6H AK = ,F7.5)
255  50 CØNTINUE
260  STØP;END
270  $DATA
```

REFERENCES

1. Chuang, S.L., "Investigation of Impact of Rigid and Elastic Bodies with Water," NSRDC Report 3248 (Feb 1970).

2. Chuang, S.L., "Theoretical Investigations on Slamming of Cone-Shaped Bodies," Journal of Ship Research (Dec 1969).

3. Chuang, S.L., "Experimental Investigation of Rigid Flat-Bottom Body Slamming," David Taylor Model Basin Report 2041 (Sep 1965).

4. Chuang, S.L., "Experiments on Slamming of Wedge-Shaped Bodies," Journal of Ship Research (Sep 1967).

INITIAL DISTRIBUTION

Copies	
8	NAVSHIPSYSCOM 2 SHIPS 2052 1 SHIPS 031 1 SHIPS 034 2 SHIPS 034-12 2 PMS 382A
11	NAVSEC 4 SEC 6110 1 SEC 6115 1 SEC 6120 1 SEC 6132 1 SEC 6139 1 SEC 6137 1 SEC 6101 1 SEC 6114D
1	ONR (Code 459)
1	NRL
2	NAVMAT 1 MAT 0331 1 MAT 033A
1	NAVORDSYSCOM ORD 913
1	NAVFACENGCOM
1	NOL Code 730
2	NWC 1 Code 556 1 Code 5056
3	CNO 1 OP 07T 1 OP 343 1 OP 723H
1	NAVAIRENGCEN
1	NAVUSYSCEN, New London
1	NELC Attn: Mr. D. Washburn
1	DNL
1	SUPSHIP 13th Naval District Code 6233D
1	CHONR (Code 439)

Copies	
1	NAVSHIPYDBSN
1	NAVSHIPYDCHASN
1	NAVSHIPYD LBEACH
1	NAVSHIPYD NORVA
1	NAVSHIPYD PEARL
1	NAVSHIPYD PTSMH
1	NAVSHIPYD BREM
1	NAVSHIPYD SFRANBAY VJO
1	Redstone Sci Info Center Chief Document Sec Attn: Mr. T.H. Duerr U.A. Army Missile Command Redstone Arsenal, Alabama 35809
1	Commander Chief Applied Mechanics Grp Attn: Tech Lib W-PAFB, Dayton, Ohio 45433
1	Commander Mechanics Div Air Force Office of Sci Research Washington, D.C. 20333
1	Commandant Chief Testing & Development Div U.S. Coast Guard 1300 E Street N.W. Washington, D.C. 20226
1	Science & Technical Div Lib of Congress Washington, D.C. 20540
1	Nat'l Sci Foundation Engr Div 1951 Constitution Ave, N.W. Washington, D.C. 20550
1	Ship Hull Research Committee Attn: Mr. A.R. Lytle Nat'l Research Council Nat'l Academy of Sciences 2101 Constitution Avenue Washington, D.C. 20418

Copies	
1	Secretary Ship Structures Committee
2	Secretary, SNAME 74 Trinity Place New York, N.Y. 10006 1 Slamming Panel
2	DDC
1	MIT, Dept of NAME Attn: Dr. A.H. Keil Cambridge, Mass 02139
1	Dept of Mechanics Lehigh Univ Bethlehem, Pa 18015
1	Lib (Code 0384) USN Post Graduate School Monterey, Calif 93940
1	Director Dept of Naval Architecture College of Engr Univ of Calif Berkeley, Calif 94720
4	Webb Inst of Naval Architecture Cresent Beach Rd Glen Cove, N.Y. 11542 1 Prof E.V. Lewis 1 Prof W.M. Maclean 1 Prof L.W. Ward
2	SWRI 8500 Culebra Rd San Antonio, Texas 78228 1 Dr. C.R. Gerlach
2	The Univ of Michigan Dept of NAME Ann Arbor, Michigan 48105 Attn: 1 Prof. H. Benford 1 Prof. F.T. Ogilvie
1	Director, Davidson Lab SIT, 711 Hudson Street, Castle Pt. Station Hoboken, N.J. 07030
1	Director Iowa Institute of Hydraulic Research, State Univ of Iowa Iowa City, Iowa

Copies	
25	JSESPO Attn Struc Br (Code F24)
3	NAVAIRSYSCOM 1 Aero & Hydro Br (Code 5301) 1 Struc Br (Code 5302) 1 Engr Div (Code 520)
1	NUWC Attn Mr. C. Miller (D602)
1	DDR & E Attn Mr. Peterson
3	Catholic Univ Washington, D.C. 1 Dean D.E. Marlowe 1 Prof M.C. Soteriades 1 Prof S.R. Heller, Jr.

UNCLASSIFIED

Security Classification

DOCUMENT CONTROL DATA - R & D

(Security classification of title, body of abstract and indexing annotation must be entered when the overall report is classified)

1 ORIGINATING ACTIVITY (Corporate author)	2a. REPORT SECURITY CLASSIFICATION
Naval Ship Research and Development Center Washington, D.C. 20034	UNCLASSIFIED
	2b. GROUP

3 REPORT TITLE

DROP TESTS OF CONES TO INVESTIGATE THE THREE-DIMENSIONAL EFFECTS OF SLAMMING

4. DESCRIPTIVE NOTES *(Type of report and inclusive dates)*

Final

5. AUTHOR(S) *(First name, middle initial, last name)*

Sheng-Lun Chuang and David T. Milne

6. REPORT DATE	7a. TOTAL NO. OF PAGES	7b. NO. OF REFS
April 1971	46	4

8a. CONTRACT OR GRANT NO.	9a. ORIGINATOR'S REPORT NUMBER(S)
Problem No. H53-007 735-073	
b. PROJECT NO.	3543
Subproject S46-06X JSESPO	
c.	9b. OTHER REPORT NO(S) *(Any other numbers that may be assigned this report)*
d. Task 1707	

10. DISTRIBUTION STATEMENT

Distribution limited to U.S. Government agencies only; Test and Evaluation Information; 29 Jan 1970. Other requests for this document must be referred to NSRDC, Code 700.

11. SUPPLEMENTARY NOTES	12. SPONSORING MILITARY ACTIVITY
	Naval Ship Systems Command and Joint Surface Effect Ships Program Office

13 ABSTRACT

Rigid-body slamming was experimentally investigated at the Naval Ship Research and Development Center by dropping one flat circular aluminum plate model and five cone-shaped aluminum models with small deadrise angles (up to 15 deg) from various elevated positions above a calm water surface. This report presents the test results and compares them with theory and to those for two-dimensional wedge-shaped models.

DD FORM 1 NOV 65 1473 (PAGE 1)

S/N 0101-807-6801

UNCLASSIFIED

Security Classification

14. KEY WORDS	LINK A		LINK B		LINK C	
	ROLE	WT	ROLE	WT	ROLE	WT
Impact of circular plate						
Impact of cone						
Impact of flat bottom						
Impact of wedge						
Ship slamming						
Trapped air phenomenon						
Three-dimensional impact						
Two-dimensional impact						
Underwater photography						